nature neuroscience

Article

https://doi.org/10.1038/s41593-025-01954-x

Aging and injury drive neuronal senescence in the dorsal root ganglia

Received: 12 January 2024

Accepted: 21 March 2025

Published online: 14 May 2025

Check for updates

Lauren J. Donovan[1] ✉, Chelsie L. Brewer[1,2], Sabrina F. Bond[1], Alexander M. Laslavic[3], Aleishai Pena Lopez[1], Laura Colman[1], Claire E. Jordan[1], Linus H. Hansen[1], Oscar C. González[2], Akshay Pujari[3], Luis de Lecea[2], Marco Quarta[3], Julie A. Kauer[2] & Vivianne L. Tawfik[1] ✉

Aging negatively impacts central nervous system function; however, there is limited information about the cellular impact of aging on peripheral nervous system function. Importantly, injury to vulnerable peripheral axons of dorsal root ganglion (DRG) neurons results in somatosensory dysfunction, such as pain, at higher rates in aged individuals. Cellular senescence is common to both aging and injury and contributes to the aged pro-inflammatory environment. We discovered DRG neuron senescence in the context of aging and pain-inducing peripheral nerve injury in young (~3 months) and aged (~24 months) male and female mice. Senescent neurons were dynamic and heterogeneous in their expression of multiple senescence markers, including pro-inflammatory factor IL6. Senescence marker-expressing neurons had nociceptor-like profiles, included high-firing phenotypes and displayed increased excitability after IL6 application. Furthermore, elimination of senescent cells resulted in improvement of nociceptive behaviors in nerve-injured mice. Finally, male and female post-mortem human DRG contained senescent neurons that increased with age (~32 years old versus 65 years old). Overall, we describe a susceptibility of the peripheral nervous system to neuronal senescence—a potential targetable mechanism to treat sensory dysfunction, such as chronic pain, particularly in aged populations.

Aging negatively impacts our physiology, with cellular-level changes influencing whole organ function. In the central nervous system (CNS), aging leads to increased risk of diseases, such as Alzheimer's and Parkinson's, which present with progressive neurodegeneration, ultimately resulting in cognitive impairments[1]. How aging impacts the peripheral nervous system (PNS) and susceptibility to sensory dysfunction, such as pain[2], remains more elusive. Limited evidence suggests alterations in primary sensory neurons with age, with few studies that investigate the cellular mechanisms that may contribute to these changes[3,4].

Cellular senescence is an aberrant state increasingly prevalent in all cells with aging. It can occur throughout the body, including in the brain and spinal cord, in response to disease or injury in young and aged animals[5,6]. Senescence is characterized by cells irreversibly ceasing cell division, resisting apoptosis and cell death and expressing a pro-inflammatory senescence-associated secretory phenotype (SASP)[7]. With age, the clearance of senescent cells decreases, resulting in their accumulation and enhanced secretion of pro-inflammatory SASP factors, ultimately contributing to the progression of age-associated disease[8]. Importantly, elimination

[1]Department of Anesthesiology, Perioperative and Pain Medicine, Stanford University, Stanford, CA, USA. [2]Department of Psychiatry and Behavioral Sciences, Stanford University, Stanford, CA, USA. [3]Rubedo Life Sciences, Inc., Sunnyvale, CA, USA. ✉e-mail: ljd14@stanford.edu; vivianne@stanford.edu

https://doi.org/10.1038/s41593-025-01954-x

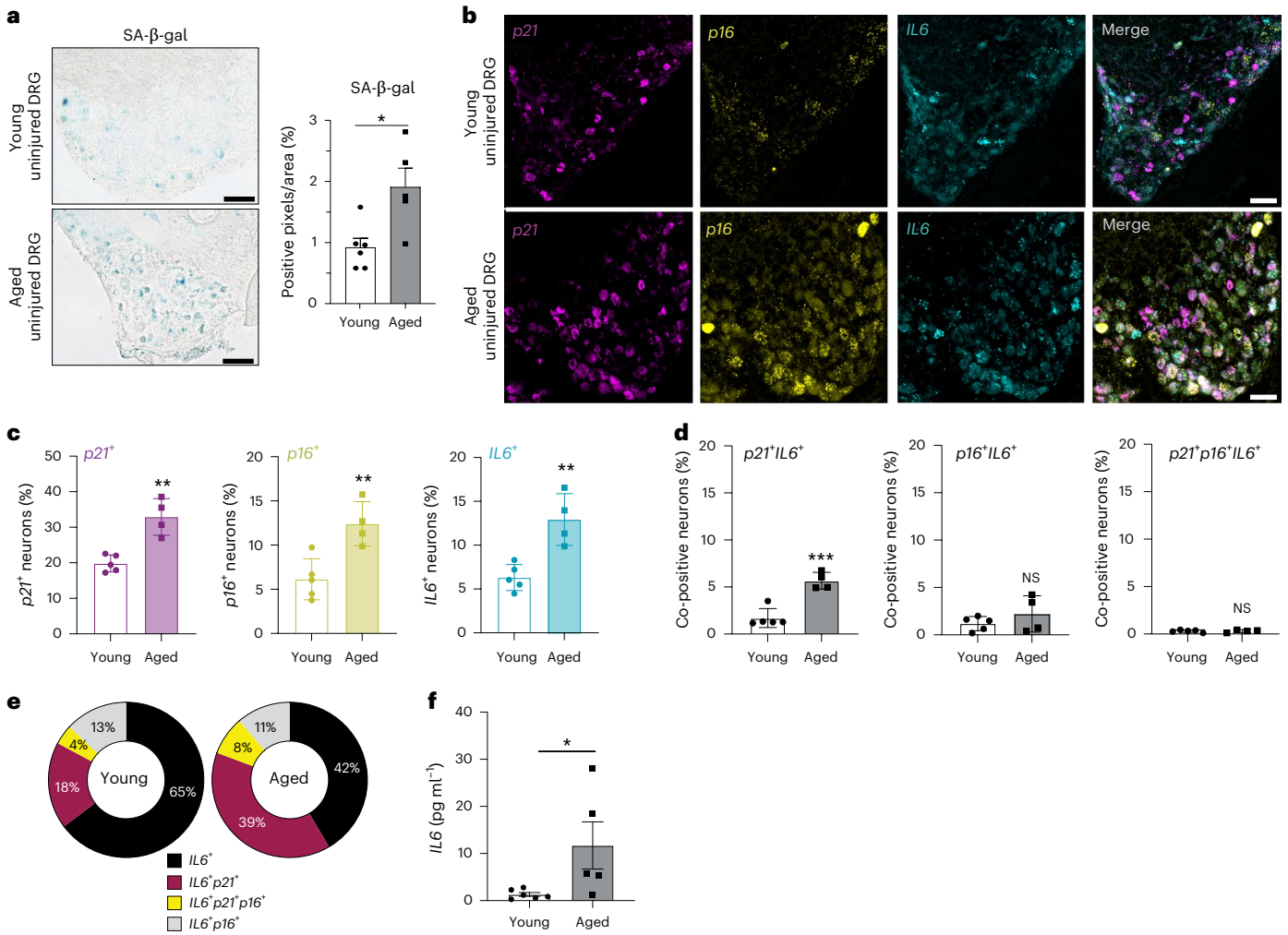

Fig. 1 | Senescent neurons accumulate with age in the mouse DRG. **a**, Representative images of SA-β-gal activity staining (blue) in the lumbar DRG of young (11–16 weeks) and aged (20–24 months) mice. Percent SA-β-gal-positive pixels per DRG area (right) ($n = 6$ young, 5 aged mice; two-tailed unpaired t-test, $P = 0.0153$). Scale bar, 100 µm. **b**, Representative RNAscope images for senescence markers *p21* and *p16* with SASP factor *IL6* in whole DRG section. Scale bar, 100 µm. **c**,**d**, Quantification of neuronal expression of each marker (**c**) or in combination (**d**) expressed as a percent of total DRG neurons ($n = 5$ young, 4 aged mice, two-tailed unpaired t-test, $p21^+$, $P = 0.0014$; $p16^+$, $P = 0.006$; $IL6^+$, $P = 0.0031$; $p21^+IL6^+$, $P = 0.0005$; $p16^+IL6^+$, $P = 0.3076$; $p21^+p16^+IL6^+$, $P = 0.1560$). **e**, Analysis of *IL6*-expressing DRG neuron population to show co-expression with senescence markers *p21* and/or *p16* in young and aged mice ($n = 5$ young, 4 aged mice). **f**, Quantification of IL6 protein levels by ELISA assay in young or aged plasma ($n = 6$ young, 5 aged mice, two-tailed unpaired t-test, $P = 0.0474$). All data are expressed as the mean ± s.e.m. NS, not significant.

of these long-lasting senescent cells improves disease pathology, underscoring their deleterious contribution to tissue function[8–10]. Cyclin-dependent kinase inhibitors $p21^{CIP1/WAF1}$ (p21) and $p16^{INK4A}$ (p16) are classic markers of senescent cells that function to halt cell cycle and drive early-stage and late-stage senescence programs, respectively[11]. Although senescence has been extensively studied in mitotic cells, there is now evidence that post-mitotic cells can acquire senescent signatures, such as expression of p21, p16 and associated SASP[12]. Intriguingly, human pyramidal and cortical neurons can express these same markers of senescence[13–15], potentially staving off neuronal loss after aberrant cell cycle entry[16]. In Alzheimer's disease, senescent neurons (and glia) are implicated in disease pathology, and genetic or pharmacologic elimination of these senescent cells in mice can improve molecular and functional outcomes[17,18]. Recently, senescent CNS neurons have gained attention as a target in the treatment of age-associated diseases[19].

Primary sensory neurons, whose cell bodies reside in the dorsal root ganglion (DRG), are susceptible to damage of their peripheral axons in a variety of contexts, including limb trauma or surgery. Injury-induced hyperexcitability of these neurons, mediated in part by chronic inflammation within the DRG, can contribute to long-lasting pain[20,21]. In particular, cytokine signaling exacerbates nociceptive neuron hyperexcitability through modulation of the Trpv1 ion channel receptor[22–24]. Interestingly, the very inflammatory molecules that mediate this hyperexcitability are all common SASP factors released by senescent cells, which may act as a potential source of these key pain-inducing molecules after injury[6].

In the present study, we identified senescent primary sensory neurons within the mouse lumbar DRG, induced with age and after peripheral nerve injury, using a comprehensive set of senescence markers, including p21 and p16, SASP factor IL6, senescence associated β-galactosidase (SA-β-gal) activity and the SenMayo[25] gene dataset, commonly used to identify senescence across various tissues. We further investigated the impact of senescence on intrinsic neuron excitability using electrophysiology and assessed pain behaviors in young and aged mice after clearance of senescent cells using a senolytic agent. Finally, we characterized senescent phenotypes in human sensory neurons with age, providing a basis for further investigation

of senescent sensory neurons in the DRG as an analgesic target in the context of age and nerve injury-induced pain.

Results

Senescent sensory neurons increase with age in the mouse DRG

We determined whether cellular senescence occurs in the PNS by examining sensory neurons in the lumbar DRG. We screened for a classic feature of senescent cells, SA-β-gal activity[7], in the DRG of young (11–16 weeks) or aged (20–24 months) male and female mice. We found an increase in SA-β-gal activity in aged compared to young DRG, indicating increased senescence of cells in the DRG with age (Fig. 1a). Based on morphology and size, most DRG cells with SA-β-gal activity were primary sensory neurons (Fig. 1a).

Although SA-β-gal activity is an indicator of senescence, its presence alone is insufficient for determining a senescent phenotype, which can be heterogeneous[7,26]. We, therefore, examined the RNA expression of two major drivers of senescence, *Cdkn2a* ($p16^{INK4A}$) and *Cdkn1a* ($p21^{WAF1/CIP1}$), in young and aged tissues by RNAscope. In aged mice, we detected significantly increased percentages of $p16^+$ neurons compared to young mice (Fig. 1b,c). Because the *Cdkn2a* transcript has two variants producing different protein products ($p16^{INK4A}$ and $p19^{ARF}$), we verified that the specific variant that produces $p16^{INK4A}$ was in fact expressed by DRG neurons (Extended Data Fig. 1). Additionally, we found an increase of $p21^+$ neurons in aged compared to young DRG (Fig. 1b,c). As deleterious senescent cells are associated with pro-inflammatory SASP, we further co-localized senescence markers, *p21* and *p16* with downstream SASP factor and cytokine *IL6*. The aged DRG displayed a significant increase in the number of $IL6^+$ as well as co-positive $p21^+IL6^+$ neurons, but not $p16^+IL6^+$ or triple-positive neurons, when compared to the young DRG (Fig. 1c,d). Interestingly, of all *IL6*-expressing neurons, a larger fraction expressed one or both senescence markers *p21* and *p16* in aged DRG (aged: 58% versus young: 35%) (Fig. 1e). Additionally, enhanced IL6 protein levels were detected in the plasma of aged versus young mice (Fig. 1f). These collective results indicate that senescent primary sensory neurons accumulate in the mouse DRG with age and express pro-inflammatory mediator and SASP factor IL6.

Nerve injury triggers neuronal senescence in the mouse DRG

We next investigated whether direct injury to peripheral axons of primary sensory neurons would increase DRG senescence in young adult mice. We performed spared nerve injury (SNI) in young mice (11–16 weeks), and lumbar L3/4 DRG were collected at multiple timepoints after SNI to evaluate senescence (Fig. 2a). We initially screened by quantitative polymerase chain reaction (qPCR) and detected a significant increase of senescence markers *p21* and *p16*, and multiple SASP factors including *IL6*, *IL1β* and *Ccl2*, in the ipsilateral SNI DRG at 3 weeks after injury compared to controls (Fig. 2b and Supplementary Table 1). To localize the cellular source of senescence marker expression in the DRG after SNI, we next performed RNAscope for *p21* and *p16* transcripts in young male and female mice at several timepoints after SNI. The majority of *p21*-expressing and *p16*-expressing cells were neurons based on cellular morphology after injury (Fig. 2c, image panels). Neurons were also confirmed as the primary senescent cell subtype after nerve injury in the DRG of young adult mice by re-analysis of a previously generated single-cell RNA sequencing (RNA-seq) dataset by Renthal et al.[27] (Fig. 2d). In our RNAscope samples, neuronal expression of senescence marker *p21* increased significantly at the early 7-day timepoint in young injured mice and remained significantly increased throughout the timecourse when compared to the young uninjured mice (Fig. 2c, upper right). In contrast, we detected a more gradual increase in the number of $p16^+$ neurons over time after injury (Fig. 2c, lower right). Very similar patterns of *p21* and *p16* gene expression after injury were revealed in the re-analysis of two independent single-cell RNA-seq DRG datasets in sciatic nerve transection (ScNT)[27] and SNI[28] nerve injury models, with a notably increasing and long-term expression of *p16* at later timepoints after nerve injury (Fig. 2e, Extended Data Fig. 2a and Supplementary Table 2). These re-analyses also showed that SenMayo genes[25], an identified reference gene set used to validate senescence via transcriptomics, were increased in DRG neurons after injury (Fig. 2e, Extended Data Fig. 2a and Supplementary Table 3). Furthermore, these analyses demonstrated that multiple subtypes of DRG neurons significantly express SenMayo genes after injury (Extended Data Fig. 2b and Supplementary Table 4).

We next tested whether senescence signatures were distinct in aged mice over time after injury. Aged DRG neurons displayed increased expression of *p21* and *p16* after injury compared to aged uninjured controls (Fig. 2f, image panels). We detected a significant, although transient, increase in the number of $p21^+$ neurons in aged mice after injury (Fig. 2f, upper right). In contrast to young mice, $p16^+$ neurons were already significantly increased in the aged DRG at 7 days and further increased and stabilized throughout the timecourse (Fig. 2f, lower right). In addition, there was a significant increase in $p21^+p16^+$ neurons in young and aged mice starting at 3 weeks after injury compared to their uninjured controls (Fig. 2g), with significantly greater numbers of senescent cells transitioning to a late-stage p16-senescent state in aged compared to young DRG (Fig. 2g).

To more robustly detect potential deleterious neuronal senescence within the DRG, we quantified the percentage of neurons that co-expressed any combination of *p21*, *p16* and downstream SASP factor *IL6* (Fig. 2h). Young, but not aged, mice accumulated significant numbers of neurons co-expressing *p21* and *IL6* in the DRG at 3 weeks after injury (Fig. 2i), suggesting a heterogeneity of senescence marker induction after injury dependent on age. Furthermore, although we did not see a significant increase in $p16^+IL6^+$ neurons after injury, we did detect an increase in triple-positive $p21^+p16^+IL6^+$ neurons in both young and aged mice, albeit in low percentages out of total DRG neurons (Fig. 2i). Finally, a majority (~65%) of all IL6-expressing DRG neurons after injury expressed *p21*, *p16* or both senescence markers in young or aged mice, a fraction of which was increased in both age groups compared to their uninjured controls (Fig. 2j compared to uninjured controls in Fig. 1e). Collectively, these data support that nerve injury drives heterogeneous senescence phenotypes in primary sensory neurons, which are a major and long-lasting cellular source of IL6 in the young and aged DRG after injury.

Injured and uninjured mouse DRG neurons express p21 and p16

We next hypothesized that neurons whose peripheral axons were injured by SNI would express senescence markers in the DRG. To test this, we co-labeled injured neurons for ATF3, a marker of axonal injury[29], as well as *p21* and *p16* at multiple timepoints after SNI. We detected very few $ATF3^+$ neurons in uninjured young or aged animals (Fig. 3a). After injury, $ATF3^+$ neurons increased to approximately 44% in the young DRG and approximately 39% in the aged DRG, of total DRG neurons (Fig. 3a and Supplementary Table 1). The majority of all $ATF3^+$ neurons co-expressed *p21* and/or *p16* in both young and aged mice (Fig. 3b, arrows, and Fig. 3c,d). We further detected a time-dependent, but age-independent, expansion of $p16^+ATF3^+$ cells, suggesting that injured neurons progressed into a *p16*-senescent state over time (Fig. 3c,d). Furthermore, not all *p21*-expressing or *p16*-expressing neurons in the DRG were $ATF3^+$ (Fig. 3b, below asterisks). The proportion of *p21*-expressing or *p16*-expressing neurons that were $ATF3^-$ either increased or remained stable over time after injury in young or aged mice (Fig. 3e,f). These results demonstrate that noninjured neurons also senesce, potentially representing 'bystander' or 'secondary' senescence in the DRG of nerve-injured mice.

To determine whether sequencing datasets captured ATF3-related senescent marker expression, we re-analyzed the DRG RNA-seq dataset from Renthal et al.[27]. We found that $ATF3^+$ DRG neurons adopt a senescent phenotype, which increases over time after injury, evident

https://doi.org/10.1038/s41593-025-01954-x

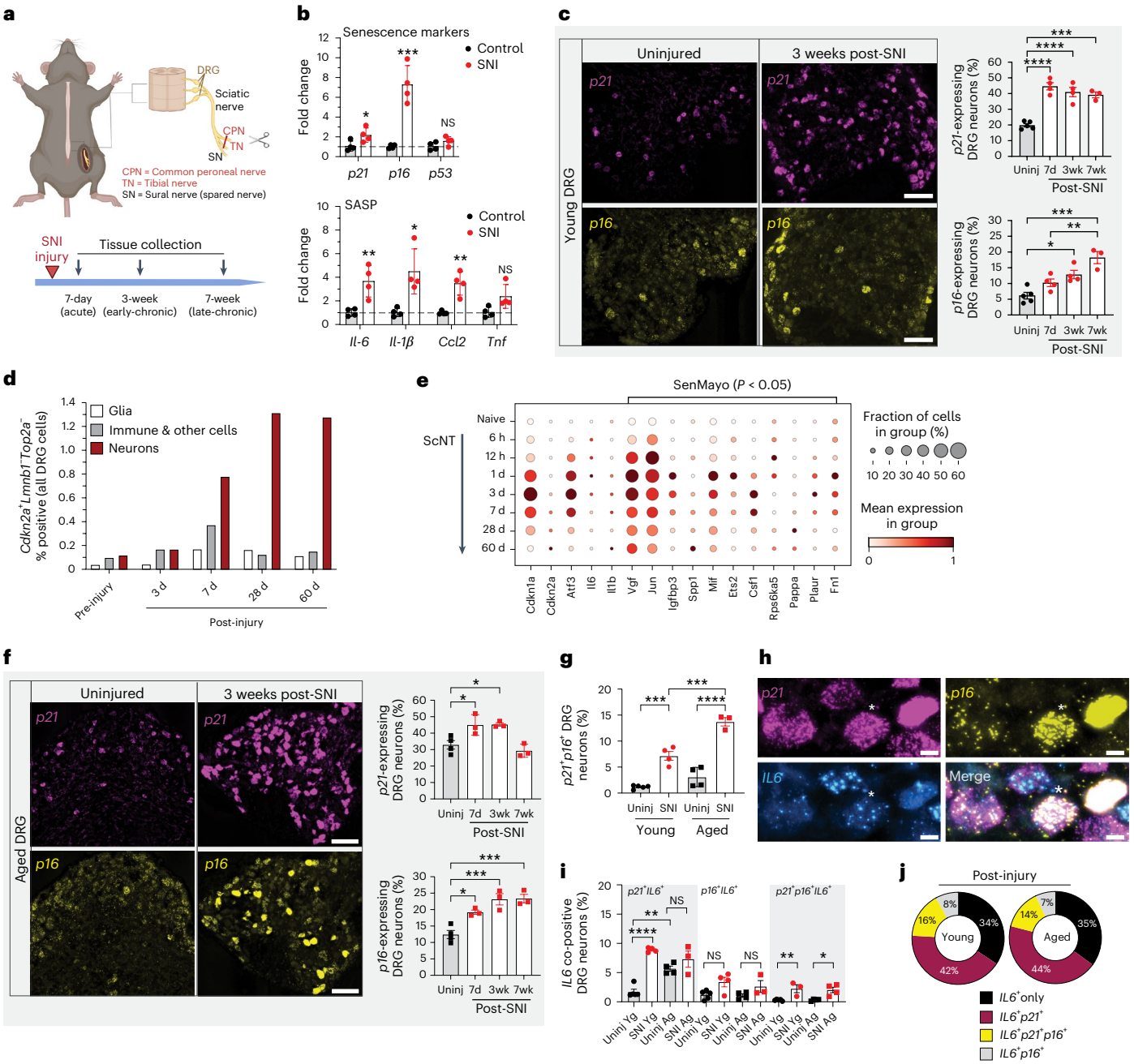

Fig. 2 | DRG neurons express senescence markers and SASP factors after peripheral nerve injury. a, Schematic of SNI and DRG tissue analysis timepoints (BioRender). **b**, qPCR from lumbar DRG in young (11–16 weeks) mice ($n = 4$ control; $n = 4$ SNI young mice; two-tailed unpaired t-test; Supplementary Table 1). **c**, Left, RNAscope image of DRG slice in young mice. Scale bar, 100 µm. Right, number of DRG neurons expressing *p21* (upper) or *p16* (lower) in young mice ($n = 5$ uninjured mice, $n = 4$, 7-day and 3-week post-SNI mice, $n = 3$, 7-week post-SNI mice; one-way ANOVA, *p21*: uninj versus 7 days or 3 weeks, $P < 0.0001$; uninj versus 7 weeks, $P = 0.0002$. *p16*: uninj versus 3 weeks, $P = 0.0117$; uninj versus 7 weeks, $P = 0.0002$; 7 days versus 7 weeks, $P = 0.0085$). **d**,**e**, Re-analysis of Renthal et al.[27]. RNA-seq dataset using young adult mouse DRG. **d**, Percentage of p16 (*Cdkn2a*$^+$)-expressing senescent cells relative to all DRG cells after ScNT. Cells are negative for *Lmnb1* and *Top2a* to filter out any nonsenescent cells. Glia, satellite glia and Schwann cells; Immune & other cells, neutrophils, macrophages, B cells, fibroblasts, endothelial cells and pericytes; Neuron, all DRG neurons. Dot plot (**e**) of senescence marker gene expression by DRG neurons after ScNT. SenMayo genes are significant, at least one timepoint (Supplementary Table 2). **f**, RNAscope image of DRG slice in aged (20–24 months) mice. Scale bar, 100 µm. Number of DRG neurons expressing either *p21* (right) or *p16* (right) in aged mice ($n = 4$ uninjured mice, $n = 3$ post-SNI mice/timepoint; one-way ANOVA, *p21*: uninj versus 7 days, $P = 0.0335$; uninj versus 3 weeks, $P = 0.0298$. *p16*: uninj versus 7 days, $P = 0.0182$; uninj versus 3 weeks, $P = 0.0009$; uninj versus 7 weeks, $P = 0.0008$). **g**, *p21*$^+$*p16*$^+$ co-expressing DRG neurons ($n = 5$ young uninjured mice, $n = 4$ young 3-week post-SNI mice; $n = 4$ aged uninjured mice, $n = 3$ aged 3-week post-SNI mice; one-way ANOVA, young uninj versus SNI, $P = 0.0002$; aged uninj versus SNI, $P < 0.0001$; young SNI versus aged SNI, $P = 0.0003$). **h**, *p21*$^+$*p16*$^+$*IL6*$^+$ (asterisk) neuron by RNAscope. Scale bar, 10 µm. **i**, *IL6*$^+$ DRG neurons co-expressing *p21* and/or *p16* ($n = 5$ young uninjured mice, $n = 4$ aged uninjured mice, $n = 4$ young 3-week post-SNI mice, $n = 3$ aged 3-week post-SNI mice; one-way ANOVA; Supplementary Table 1). **j**, *IL6*$^+$ DRG neurons co-express *p21* and/or *p16* at 3 weeks after SNI ($n = 3$ mice per group). All data are mean values ± s.e.m. Ag, aged; d, days; h, hours; NS, not significant; wk, weeks; Yg, young.

https://doi.org/10.1038/s41593-025-01954-x

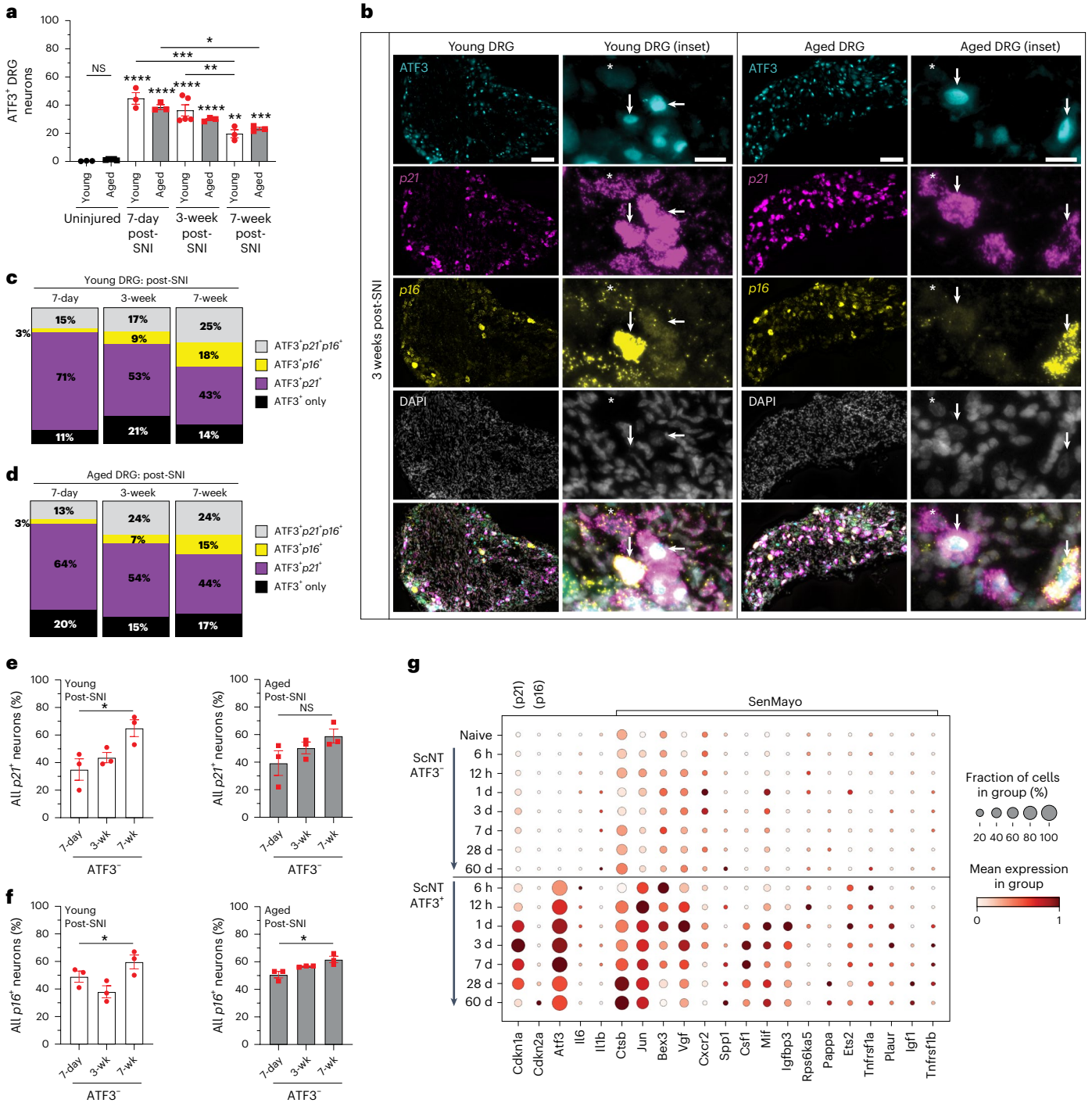

Fig. 3 | ATF3⁺ injured and neighboring noninjured DRG neurons express senescence markers after nerve injury. a, Quantification of number of ATF3⁺ neurons as a percent of total L3/4 DRG neurons in uninjured and multiple post-SNI timepoints in young (11–16 weeks) and aged (20–24 months) mice ($n = 3$ young, $n = 5$ aged uninjured mice; $n = 3$ 7-day post-SNI mice/age group; $n = 5$ young, $n = 3$ aged 3-week post-SNI mice; $n = 3$ 7-week post-SNI mice/age group, one-way ANOVA; see Supplementary Table 1 for all P values). Data are mean values ± s.e.m. **b**, Representative images of dual immunohistochemistry/RNAscope labeling ATF3⁺ injured neurons (nuclear-localized protein) and RNA puncta of p21 and p16 at 3 weeks after SNI. Co-expression of ATF3 with *p21* and or *p16* (arrows). Asterisks represent ATF3⁻ cells that express p21 and/or p16 senescence markers. Scale bar, 100 µm. Inset scale bar, 20 µm. **c**,**d**, Quantification of ATF3⁺ neuron population that co-express *p21* and/or *p16* at multiple timepoints after injury in young and aged DRG (young: $n = 3$–5 mice per timepoint per group: 7-day: $n = 1{,}421$ ATF3⁺ neurons, 3-week: $n = 1{,}056$ ATF3⁺ neurons; 7-week: $n = 523$ ATF3⁺ neurons; aged: $n = 3$ mice per timepoint: 7-day: $n = 1{,}004$ ATF3⁺ neurons; 3-week: $n = 983$ ATF3⁺ neurons; 7-week: $n = 722$ ATF3⁺ neurons). **e**, Quantification of ATF3⁻ population co-expressing senescence marker *p21* at multiple timepoints after injury in young and aged DRG ($n = 3$ mice per group per timepoint, one-way ANOVA, young, $P = 0.0323$; aged, $P = 0.1761$). Data are mean values ± s.e.m. **f**, Quantification of ATF3⁻ population co-expressing senescence marker *p16* at multiple timepoints after injury in young and aged DRG ($n = 3$ mice per group per timepoint, one-way ANOVA, young, $P = 0.0397$; aged, $P = 0.0188$). All data are expressed as the mean ± s.e.m. **g**, Re-analysis of Renthal et al.[27]. RNA-seq dataset from young adult mouse DRG. Dot plot demonstrates the timecourse of senescence marker gene expression after ScNT by either ATF3⁻ (top) or ATF3⁺ (bottom) DRG neurons (Supplementary Table 3). NS, not significant; wk, week.

https://doi.org/10.1038/s41593-025-01954-x

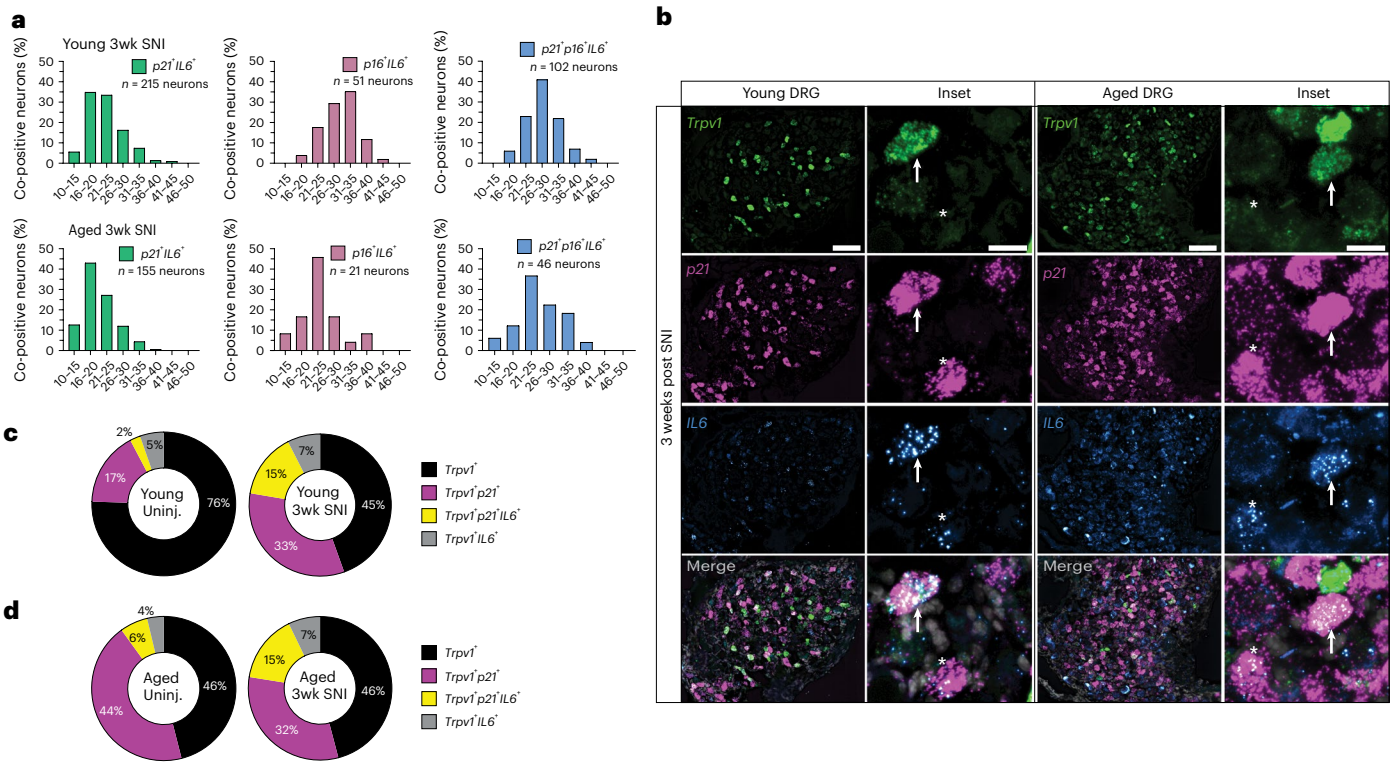

Fig. 4 | Trpv1$^+$ nociceptors express senescence markers after nerve injury. **a**, Analysis of cell diameter (μm) of *p21*$^+$*IL6*$^+$, *p16*$^+$*IL6*$^+$ or *p21*$^+$*p16*$^+$*IL6*$^+$ co-positive neurons in the DRG at 3 weeks after nerve injury in young (11–16 weeks) and aged (20–24 months) mice (young: $n = 215$ *p21*$^+$*IL6*$^+$ neurons; $n = 51$ *p16*$^+$*IL6*$^+$ neurons; $n = 102$ *p21*$^+$*p16*$^+$*IL6*$^+$ neurons; aged: $n = 155$ *p21*$^+$*IL6*$^+$ neurons; $n = 21$ *p16*$^+$*IL6*$^+$ neurons; $n = 46$ *p21*$^+$*p16*$^+$*IL6*$^+$ neurons). **b**, Representative RNAscope images of young or aged DRG co-labeled for the ion channel Trpv1, senescence marker p21 and SASP factor/cytokine IL6. Merged images also have DAPI overlay (gray). For *IL6* signal, intense puncta signal with white center are positive neurons, and fainter/dull blue is background. Arrows: *Trpv1*$^+$ senescent neurons; asterisks: *Trpv1*$^-$ senescent neurons. Scale bars, 100 μm and 20 μm (insets). **c**,**d**, Quantification of *Trpv1* neuron population and its co-expression with *p21* and/or *IL6* in young (**c**) and aged (**d**) L3/4 DRG of uninjured (controls) and 3 weeks after SNI ($n = 3$ uninjured young mice, $n = 972$ *Trpv1*$^+$ neurons; $n = 3$ SNI young mice, $n = 1{,}548$ *Trpv1*$^+$ neurons; $n = 4$ uninjured aged mice, $n = 1{,}056$ *Trpv1*$^+$ neurons; $n = 3$ SNI aged mice, $n = 1{,}292$ *Trpv1*$^+$ neurons). wk, weeks.

by increased *p21* (*Cdkn1a*) and *p16* (*Cdkn2a*) expression (Fig. 3g). In addition, ATF3$^+$ neurons significantly upregulated several SenMayo genes after injury (Fig. 3g and Supplementary Table 5). Although a more minor signature, some ATF3$^-$ neurons also expressed these markers of senescence after injury, together replicating our findings in an independent dataset (Fig. 3g and Supplementary Table 5).

Nociceptors express senescence markers in the mouse DRG

Individual subtypes of sensory neurons are distinct in size, tuned to respond to unique stimuli and vary in their expression of canonical markers[30]. To identify the subtype(s) of primary sensory neurons that express senescence markers after nerve injury, we analyzed their cell diameters. In our dataset, the majority of *p21*$^+$*IL6*$^+$ neurons measured in the range of 16–30 μm, with a mean diameter of 22 μm (±5.49 μm) in young mice and 20 μm (±4.96 μm) in aged mice (Fig. 4a). In comparison, *p16*$^+$*IL6*$^+$ neurons were slightly larger in diameter, with a mean diameter of 29 μm (±5.51 μm) in young mice and 24 μm (±5.96 μm) in aged mice (Fig. 4a). In either case, young or aged IL6-expressing senescent neurons were rarely of large diameter (Fig. 4a).

Given that the majority of neurons expressing senescence markers with SASP factor IL6 were small diameter, we theorized that these senescent neurons may be Trpv1$^+$, as this ion channel is widely expressed in small-diameter nociceptive neurons[24,31]. To identify whether these *Trpv1*$^+$ neurons localized with senescence markers (*p21* and *p16*) and IL6, we co-labeled these neurons at baseline (uninjured) and after SNI (Fig. 4b). We found an expansion of *Trpv1*$^+$*p21*$^+$ and *Trpv1*$^+$*p21*$^+$*IL6*$^+$ neurons in both young and aged DRG at 3 weeks after SNI (Fig. 4c,d). Taken together, these data support enhanced *Trpv1*$^+$ nociceptor senescence with age and after injury, with an increased fraction that co-express *IL6* after injury in both young and aged mice.

Senescent mouse neurons include IL6-responsive nociceptors

Next, we investigated the electrophysiological properties of senescent neurons to characterize their function in the DRG. We used whole-cell patch-clamp recordings in intact DRG preparations from young (11–16 weeks) and aged (20–24 months) mice with and without injury, followed by single-cell PCR to detect *p16*, *p21* and *IL6*.

We recorded from 82 lumbar DRG neurons from 26 mice. Given the heterogeneity of DRG functional profiles, we employed dimensionality reduction using uniform manifold approximation and projection (UMAP; Python implementation from https://github.com/lmcinnes/umap) based on 33 parameters collected during recordings, including firing properties, diameter and intrinsic currents (Fig. 5a). This analysis produced five discrete clusters determined by a hierarchical density-based cluster algorithm (HDBSCAN; Python implementation from https://github.com/scikit-learn-contrib/hdbscan; Fig. 5b). We analyzed the distribution of senescence markers (*p21*: Fig. 5c; *p16*: Fig. 5d; and *IL6*: Fig. 5e) within the clusters. Notably, the majority of *p16*-expressing neurons localized to cluster 5 (83%, 5/6), a cluster that contained all neurons with high evoked firing phenotypes (defined as >100 action potentials (APs) fired during all current steps; Fig. 5f, top heatmap), and two of the high-firing neurons were *p16*$^+$ (Fig. 5f, top and lower left heatmap). Similarly, most *IL6*-expressing neurons were found in cluster 5 (Fig. 5e) and included a high-firing phenotype neuron (13%, 1/8; Fig. 5f, top and lower left heatmap). Cluster 5 also contained neurons with lower rheobase (Fig. 5f, top and lower right

https://doi.org/10.1038/s41593-025-01954-x

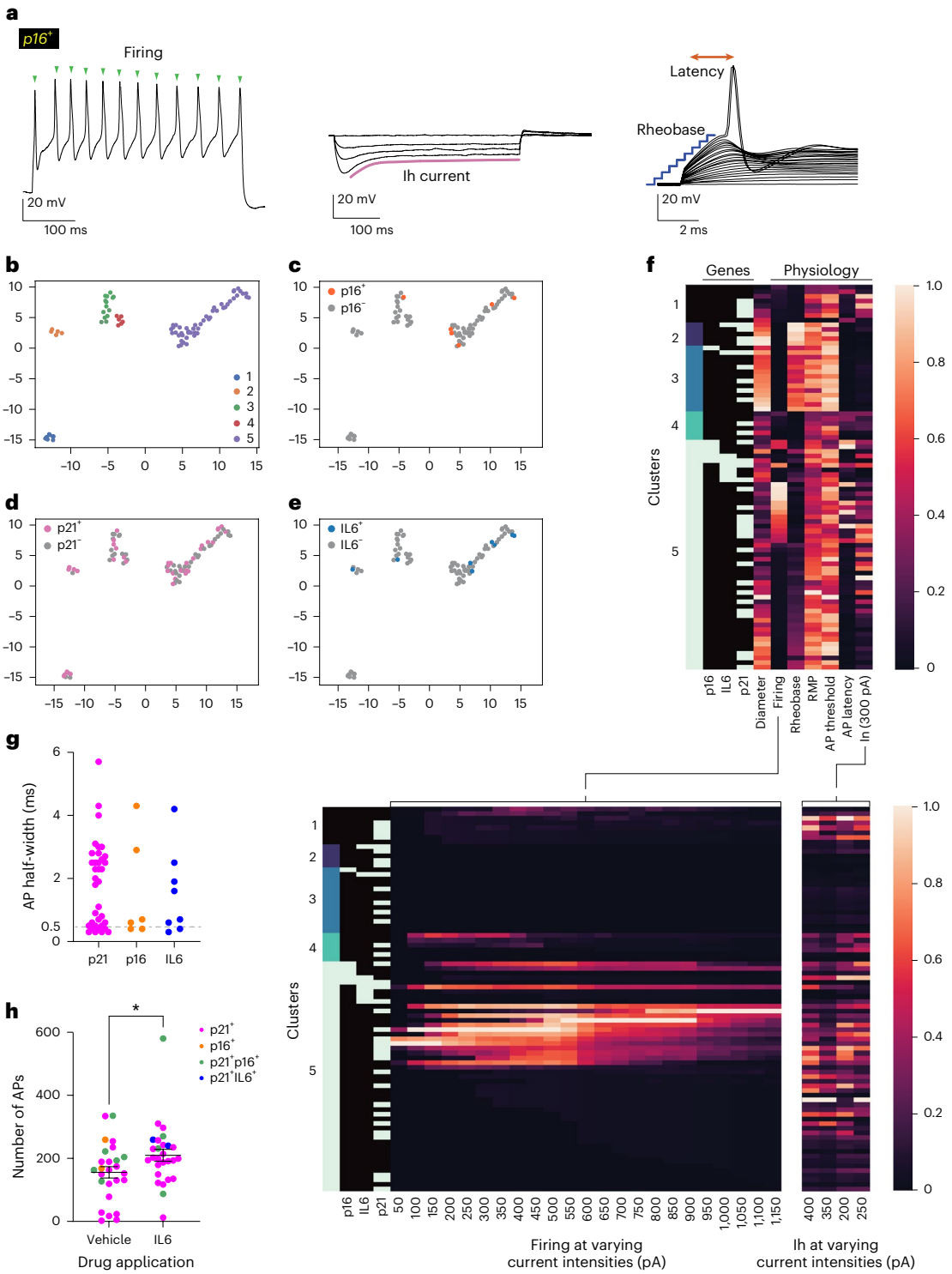

Fig. 5 | DRG neurons expressing senescence and SASP markers include high-firing and nociceptor-like phenotypes, and the SASP factor IL6 increases excitability in these populations. a, Representative traces from *p16*-expressing neurons demonstrating repetitive firing (left), hyperpolarization-activated current (Ih) presence (middle) and the firing parameters rheobase and AP latency (right). **b**, Clusters identified with the hierarchical density-based algorithm HDBSCAN after UMAP alignment of individual neurons constructed with diameter (range, 14–41 µm), firing properties and intrinsic currents. Discrete clusters[1–5] are identified by color ($n = 82$ recorded DRG neurons from young (11–16 weeks) and aged (20–24 months) mice). UMAP highlighting senescence marker *p16* (orange) (**c**), *p21* (pink) (**d**) and the SASP factor *IL6* (blue) (**e**). **f**, Heatmap depicting parameters from left to right as follows: clusters (cool gradient), gene expression (black, no expression; light teal, expression), diameter and physiology parameters (warm gradient; higher normalized values are lighter and lower values are darker). Senescence marker *p16* and SASP factor *IL6* groups contain neurons with high-firing phenotypes (>100 total APs fired during current steps), which is outlined over increasing depolarizing current steps (lower left panel). Ih current amplitude was also measured at decreasing hyperpolarizing steps (lower right panel). **g**, Senescent neurons (p21 in magenta, p16 in orange and IL6 in blue) display the DRG nociceptor-associated property of wide APs (half-width above 0.5 ms, gray dotted line). **h**, IL6 application increases evoked firing in senescence marker-expressing neurons in monolayer culture (155.5 ± 18 APs, $n = 26$ cells from 11 mice for control; 209.7 ± 19.06 APs, $n = 27$ cells from 13 mice for IL6 application; $U = 234.5$, $P = 0.038$, two-sided, Mann–Whitney test; neuronal expression of p21 in magenta, p16 in orange, p21 and p16 in green and p21 and IL6 in blue). All data are mean values ± s.e.m.

https://doi.org/10.1038/s41593-025-01954-x

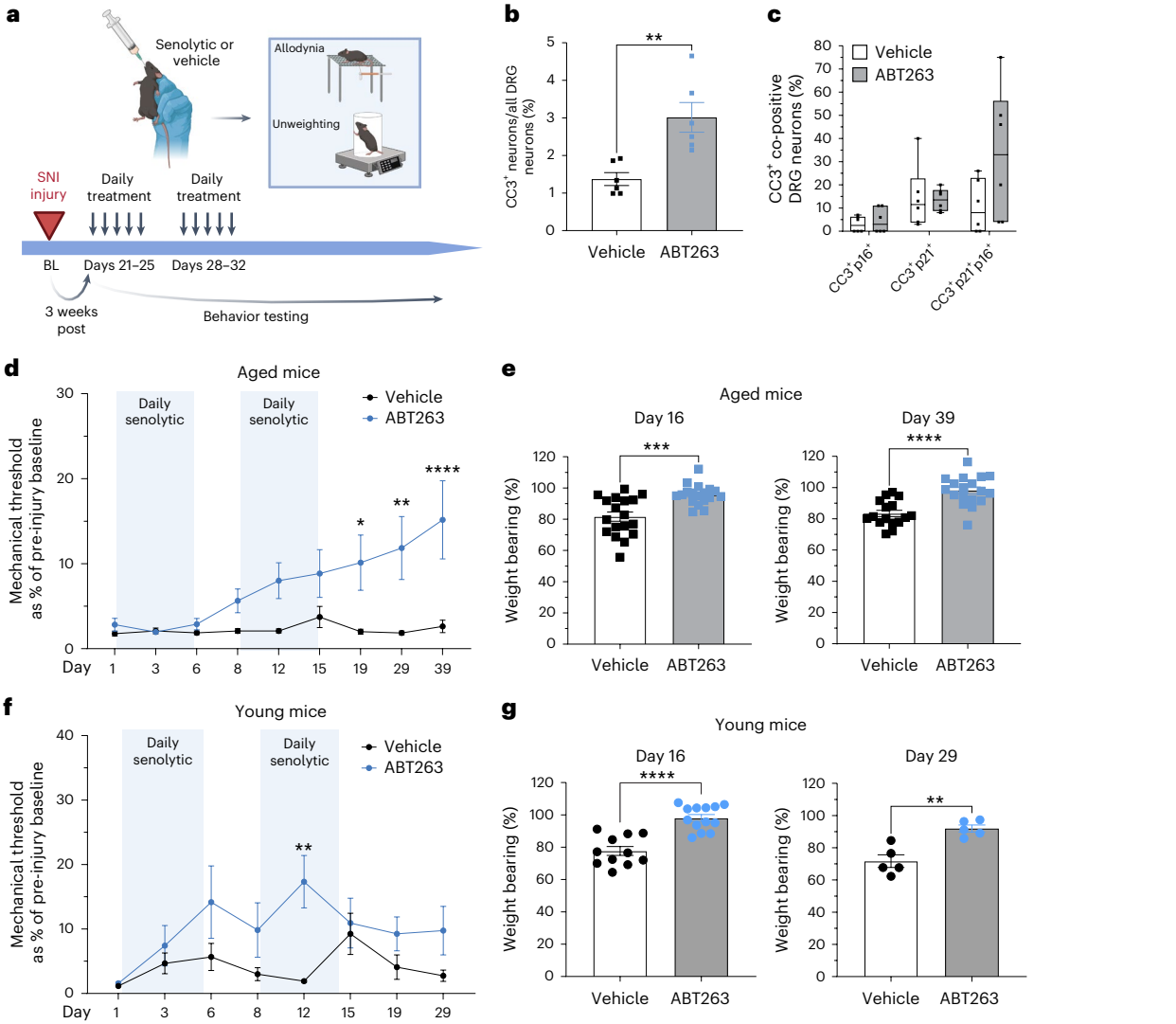

Fig. 6 | In vivo elimination of senescent neurons using senolytics alleviates pain behaviors after nerve injury. a, Schematic of treatment paradigm (BioRender). Young (11–16 weeks) and aged (20–24 months) mice were treated with senolytic (ABT263, 100 mg kg^{-1}) or vehicle for 10 days by oral gavage, starting at 3 weeks after SNI. Mechanical allodynia and weight bearing were assessed during and after treatment. **b**, Quantification of CC3$^+$ neurons in the DRG after treatment with vehicle or ABT263 for five consecutive days ($n = 3$ male, $n = 3$ female aged mice per treatment group, two-tailed unpaired t-test, $P = 0.0034$). **c**, CC3$^+$ neurons analyzed for their co-expression with p21 and/or p16 senescence markers. Categories are mutually exclusive ($n = 3$ male, $n = 3$ female aged mice per treatment group; data show minimum to maximum, all points). **d**, Aged mice treated with ABT263 or vehicle (light blue indicates treatment window) and their mechanical allodynia thresholds were assessed ($n = 12$ female, $n = 10$ male vehicle-treated mice; $n = 15$ female, $n = 13$ male ABT263-treated mice, mixed effects analysis, two-sided, Sidak's multiple comparisons test, day 19, $P = 0.0309$; day 29, $P = 0.0033$; day 39, $P < 0.001$). **e**, Aged mice treated with ABT263 displayed improved weight bearing on injured limb compared to vehicle-treated mice at both day 16 ($n = 10$ female, $n = 8$ male vehicle-treated mice; $n = 9$ female, $n = 9$ male ABT263-treated mice, two-tailed unpaired t-test, $P = 0.0002$) and day 39 ($n = 9$ female, $n = 7$ male vehicle-treated mice; $n = 9$ female, $n = 9$ male ABT263-treated mice, two-tailed unpaired t-test, $P < 0.0001$) after treatment start. **f**, Young mice were treated with ABT263 or vehicle (light blue indicates treatment window), and their mechanical allodynia thresholds were assessed ($n = 12$ male vehicle-treated mice, $n = 12$ male ABT263-treated mice, two-way ANOVA, two-sided, Sidak's multiple comparisons test, day 12, $P = 0.0018$). **g**, Young mice treated with ABT263 displayed improved weight bearing on injured limb compared to vehicle-treated mice at both day 16 ($n = 11$ vehicle-treated, $n = 13$ ABT263-treated male mice, two-tailed unpaired t-test, day 16, $P < 0.0001$) and day 29 ($n = 5$ vehicle-treated, $n = 5$ ABT263-treated male mice, two-tailed unpaired t-test; day 29, $P = 0.002$) after treatment start. All data are mean values ± s.e.m. BL, baseline.

heatmap), suggesting increased excitability[32]. *p21*-expressing neurons, however, encompassed a larger population and were distributed throughout all clusters (Fig. 5d,f). Overall, the majority of high-firing neurons expressed at least one senescence marker (63%, 10/16; Fig. 5f). Additionally, senescence marker and/or SASP factor-expressing populations contained neurons with wide APs (defined as AP half-widths greater than 0.5 ms; *p16*: 67%, 4/6; *p21*: 72%, 26/36; *IL6*: 75%, 6/8; Fig. 5g), suggesting that they belong to nociceptor or C-fiber low-threshold mechanoreceptor classes, which express Trpv1 (ref. 33), supporting our findings that Trpv1$^+$ nociceptors senesce. Together, these data suggest that senescence marker-expressing DRG contain populations of high-responding DRG neurons and share physiological characteristics with nociceptors, supporting a direct contribution to heightened excitability in the DRG.

To address whether senescence marker-expressing neurons are responsive to cytokine/SASP factor IL6, we cultured aged DRG neurons and measured their excitability in response to exposure to vehicle or IL6 via whole-cell patch-clamp recording, and we post hoc identified their

identity via qPCR (Fig. 5h). We found that cultured aged DRG neurons expressed senescence markers alone or in combination and included *p21*$^+$, *p16*$^+$, *p21*$^+$*p16*$^+$ or *p21*$^+$*IL6*$^+$ neurons. We found a significant increase in the number of APs fired by senescence marker-expressing neurons after IL6 application (n = 27 cells from 13 mice) when compared to vehicle-treated (n = 26 cells from 11 mice; P = 0.038, Mann–Whitney test). The majority of responding neurons were *IL6*$^-$, demonstrating that paracrine action of IL6 onto senescence marker-expressing neurons is possible. Collectively, these results demonstrate that senescent DRG neurons can indirectly increase the excitability of the DRG through their production of the SASP factor *IL6*.

Senescent cell removal improves pain behaviors in aged mice

We next hypothesized that clearance of senescent DRG neurons would improve pain behaviors induced by SNI. We tested ABT263 (Navitoclax), a peripherally restricted senolytic that promotes apoptosis of senescent cells[34,35]. We treated mice with ABT263 (100 mg kg^{-1}, oral gavage) or vehicle for 10 days starting at 3 weeks after SNI, a timepoint at which senescent neurons have accumulated in young and aged mice (Fig. 6a). Treatment with ABT263 induced apoptosis of DRG neurons, as evidenced by a significant increase in the number of cleaved caspase-3-positive (CC3$^+$) (that is, apoptotic) neurons (Fig. 6b and Extended Data Fig. 3a). Additionally, a higher fraction of CC3$^+$ neurons co-expressed both senescence markers *p16* and *p21* in ABT263-treated mice (Fig. 6c and Extended Data Fig. 3b). In aged mice treated with ABT263, we observed a gradual improvement in mechanical allodynia up to at least approximately 3 weeks after treatment (Fig. 6d). In addition, aged mice showed a significant improvement in weight bearing immediately (day 16) and 3 weeks (day 39) after senolytic treatment (Fig. 6e). In young mice, there was only a transient increase in mechanical threshold after ABT263 treatment (Fig. 6f); however, we did detect sustained improvement in weight bearing (Fig. 6g). Sensory function of the contralateral (uninjured) hindlimb and motor function were not altered after application of senolytics in aged or young mice (Extended Data Fig. 3c–e). Collectively, these data show that senescent DRG neurons can be targeted by senolytics and that treatment can improve pain-like behaviors more effectively in aged animals.

Human DRG neurons accumulate senescence markers with age

To validate the translational potential of senescent cell subpopulations as a target in humans, we assessed senescent marker expression in human DRG neurons. As it is difficult to obtain postmortem human DRG tissues with confirmed injury/damaged nerves, we evaluated whether senescence markers increase with age. We collected L4 DRG from two young (32-year-old and 33-year-old) female and two aged (both 65-year-old) male and female human donors and examined senescence marker expression by RNAscope. Similar to mice, human DRG neurons clearly expressed *p21* and *p16* (Fig. 7a,b), which were increased in aged DRG (Fig. 7c). Furthermore, greater numbers of *IL6*$^+$ neurons were detected in aged compared to young human DRG (51.8% aged versus 22.7% young) (Fig. 7d). Of this *IL6*-expressing neuronal population, aged DRG had an increased fraction and total neurons that co-expressed either *p21* or *p16*, with a striking increase in triple-positive cells (*IL6*$^+$*p21*$^+$*p16*$^+$: 51% aged versus 33% young) (Fig. 7e,f). We observed that human DRG neurons had higher amounts of lipofuscin (a marker of lysosomal impairment and senescence[36]), with an increased fraction of neurons >75% lipofuscin-filled in the aged DRG, occluding the RNAscope signal and precluding further analysis of additional senescence marker expression (Extended Data Fig. 4a,b).

We next asked whether injured (ATF3$^+$) human sensory neurons existed in the young and aged human DRG. We detected a similar number of ATF3$^+$ neurons in young and aged human L4 DRG tissues (Fig. 7g); however, a greater percent co-expressed *p21* in aged (97%) compared to young (82%) human DRG (Fig. 7h).

To extend our analyses to additional human DRG across ages and associated with pain states, we re-analyzed two publicly available human DRG RNA-seq datasets (Extended Data Fig. 5 and Supplementary Table 1). First, re-analyzing a single-cell RNA-seq dataset[37], we detected an age-related increase in the percentage of DRG neurons expressing *p16* as well as *p21* when comparing three human DRG samples (ages 23, 56 and 61 years) (Extended Data Fig. 5a,b). Furthermore, we confirmed the co-expression of ATF3$^+$ neurons with *p21* and *p16*, which also showed an age-related increase in number for all subtypes (Extended Data Fig. 5c). In a separate re-analysis of a bulk RNA-seq dataset generated using excised DRG collected from patients with or without at-level pain[38], we found a significant correlation between increased *CDKN2A* (p16) expression and age (Extended Data Fig. 5d; Spearman correlation coefficient = 0.612, P = 0.00321). We also discovered a significant association of SenMayo gene expression specifically in 'pain' DRG samples compared to the 'no pain' condition (t-test, P = 0.0182) (Extended Data Fig. 5e and Supplementary Table 1). These data together replicated our findings of an age-related increase of senescent neurons in the human DRG as well as demonstrated an association between pain and senescence marker expression.

To characterize sensory neurons susceptible to age-induced senescence in humans, we next analyzed neuron diameter. Similar to mouse DRG neurons, senescence marker-expressing human DRG neurons were generally of small diameter in both young and aged DRG (Extended Data Fig. 6a,b). Finally, we detected that approximately 64.6% of all young and approximately 64.0% of all aged L4 DRG neurons expressed *TRPV1* (Fig. 7i, left). Of these *TRPV1*$^+$ neurons, we found a higher fraction co-expressing either *p16* or *p21* in aged versus young DRG (Fig. 7i, right box, and Fig. 7j). Furthermore, we observed a shift in *TRPV1*$^+$ nociceptor co-expression with *p21* and *p16*, with a majority of *TRPV1*$^+$ neurons (91%) expressing one or both markers in the aged DRG compared to young DRG (67%) (Fig. 7j,k). These data collectively show that human DRG

Fig. 7 | Human DRG neurons express senescence markers and SASP factor IL6 with age. a,**b**, Representative RNAscope images from young or aged human L4 DRG showing expression of *p21* and *p16* senescence markers (enlarged left images with DAPI; scale bar, 100 µm). The large globular signal present in both channels is autofluorescent lipofuscin and not RNAscope signal (small puncta). **c**, Quantification of *p21*$^+$ and *p16*$^+$ neurons in the young and aged human DRG as a percent of total DRG neurons (n = 2 young female (32-year-old and 33-year-old); n = 2 aged male/female (65-year-old) DRG). **d**, Quantification of *IL6*-expressing neurons as a percent of total DRG neurons (n = 2 young female (32-year-old and 33-year-old); n = 2 aged male/female (65-year-old) DRG). **e**, Analysis of *IL6*$^+$ neuron population and quantification of the co-expression of senescence markers *p21* and/or *p16*. **f**, Quantification of neurons co-expressing senescence markers *p21* and/or *p16* with *IL6* as a percent of total DRG neurons (n = 2 young female (32-year-old and 33-year-old); n = 2 aged male/female (65-year-old) DRG). **g**, Percent of DRG neurons that are ATF3$^+$ in young and aged human DRG (n = 2 young female (32-year-old and 33-year-old); n = 2 aged male/female (65-year-old) DRG). **h**, Example image depicting a single human neuron positive for ATF3 (nuclear-localized, immunohistochemistry) and *p21* (RNAscope, puncta). Scale bars, 20 µm. Analysis of ATF3$^+$ neuron population and quantification of the co-expression with p21 in young and aged human DRG (right, donuts) (n = 64 young ATF3$^+$ DRG neurons, n = 54 aged ATF3$^+$ DRG neurons). **i**, Total percentage of *TRPV1*$^+$ neurons as a percent of total DRG neurons in young and aged human DRG. Quantification of the subsets of *TRPV1*$^+$ neurons that co-express either *p21* or *p16* by RNAscope (boxed right) (n = 2 young female (32-year-old and 33-year-old); n = 2 aged male/female (65-year-old) DRG). **j**, Single representative human neurons (quantified in **k**) showing co-expression of *TRPV1* with *p21* and/or *p16*. DAPI in gray. Scale bars, 20 µm. **k**, Venn diagram of human DRG neurons that express *TRPV1*, *p16* and *p21*. Aged DRG display a greater overlapping fraction of *TRPV1*$^+$ neurons expressing either or both senescence markers *p21* and *p16* compared to young neurons. n = 2 young female (32-year-old and 33-year-old); n = 2 aged male/female (65-year-old) DRG. All data are mean values ± s.e.m.

https://doi.org/10.1038/s41593-025-01954-x

neurons senesce with age, including injured ATF3$^+$ and TRPV1$^+$ neurons, and that senescent neurons are a source of IL6 in the aging human DRG.

Discussion

Using several complementary approaches, we show that primary sensory neurons senesce with age and after peripheral nerve injury and that targeting these neurons can improve sensory dysfunction. First, we discovered an age-associated increase in the neuronal expression of key senescence markers, including *p21* and *p16*, as well as SASP component IL6 when comparing aged (20–24 months) to young (11–16 weeks) mouse DRG, which was further increased after peripheral injury. This is in agreement with prior work showing that other tissues throughout the body accumulate senescent cells with chronological age[6]. We validated this key concept in human DRG, providing evidence of senescence in human primary sensory neurons. Supporting our findings of DRG neuronal senescence, re-analysis of existing DRG RNA-seq datasets

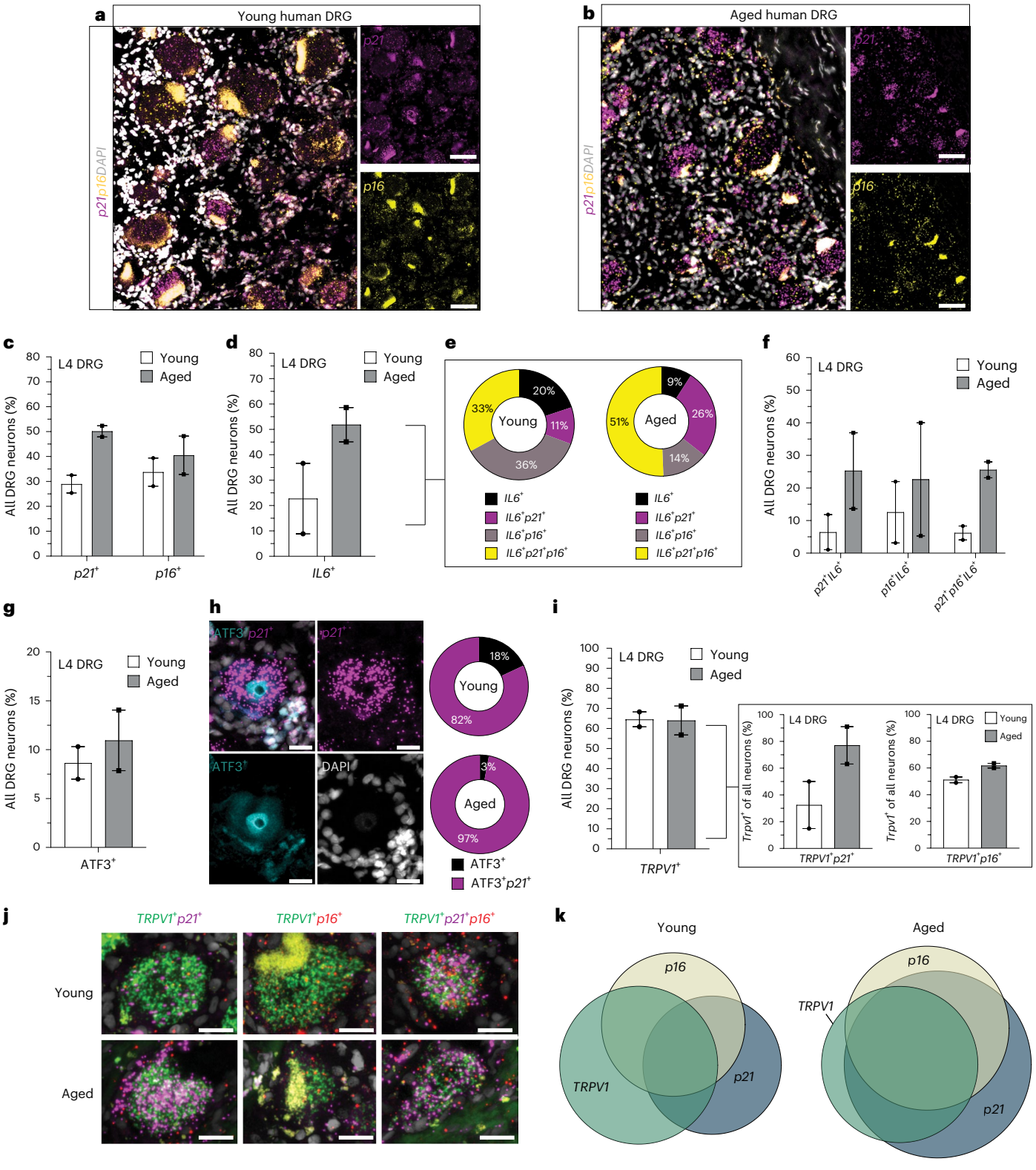

identified sensory neurons as the primary DRG cell type senescing after nerve injury. A recently published re-analysis study also provides support for our proposed hypothesis[39]. In addition, unbiased clustering of senescence marker-positive neurons based on their electrophysiology parameters characterized these cells as high-responding DRG neurons, and application of IL6 increased the evoked firing of senescence marker-expressing DRG. Lastly, DRG neurons targeted in vivo by a senolytic ABT263 (Navitoclax) resulted in improved mechanical allodynia and weight bearing on the injured hindlimb, without sensory or motor deficits.

The concept of neuronal senescence is an emerging one, as the classic hallmark senescence feature of cell cycle arrest is generally thought to be absent in post-mitotic cell types. However, multiple features of senescence can be present in post-mitotic cells, including expression of cyclin-dependent kinase inhibitors (p21 and p16), SA-β-gal activity, DNA damage/oxidative stress markers and SASP component expression[40]. Such findings in the CNS prompted a new term, 'postmitotic cellular senescence' (PoMiCS), to complement this observed phenotype, with SASP being an important detrimental feature of post-mitotic senescent cells[40,41]. Why would post-mitotic cells such as neurons upregulate cyclin-dependent kinase inhibitors p21 or p16? In neurodegenerative conditions, neurons aberrantly re-enter the cell cycle in response to cellular stress, which can lead to cell death of damaged neurons[42,43]. Expressing cyclin-dependent kinase inhibitors (p21 and p16) would, therefore, halt the cell cycle, induce senescence and ultimately stave off apoptosis to preserve neuronal numbers[16,40]. Depending on the context, however, it may not be beneficial to preserve neurons that are damaged; transient senescence may be beneficial, whereas persistent senescence may cause dysfunction[44]. Primary sensory neurons may undergo a similar stress response mechanism of cell cycle re-entry upon nerve injury, resulting in post-mitotic cellular senescence. Indeed, DRG neurons can re-enter the cell cycle in response to other stressors, such as growth factor restriction and chemotherapy[45,46].

The SNI model of neuropathic pain used in this study provides a unique opportunity to study neuronal senescence with spatiotemporal control. This is in contrast to investigating senescence in slowly progressing disease models such as Alzheimer's[17,18]. Using this spatially restricted and injury-triggered induction of senescence, we were able to track neuronal senescent phenotypes over time after nerve injury and identify characteristics distinct during aging in both injured and uninjured neurons. Over the post-injury timecourse, we captured a phenotypic shift (that is, p21-to-p16 expression) of DRG neurons. Specifically, in the young DRG, we detected an early spike in $p21^+$ neurons that declined over time, whereas the $p16^+$ neuron population gradually increased over time. Similarly in human fibroblasts, p21 expression was found to decrease after senescence was achieved, followed by subsequent upregulation of p16 expression to maintain senescent cell cycle arrest[11]. Interestingly, aged neurons progress to late-stage senescence quicker compared to young neurons as evidenced by p16 expression at earlier timepoints. Both injured and noninjured neurons expressed senescence markers over time after injury, suggesting that this model captures a heterogenous population of (1) age-induced ongoing primary senescence; (2) primary senescence, induced directly by the cell stressor (axon injury); and (3) secondary 'bystander' senescence, induced by paracrine action of SASP-producing primary senescent cells[47]. In support of this, the population of senescent neurons that were $ATF3^-$ (noninjured) increased over time in young and aged animals after injury. Additionally, senescence of other cells such as glia in the DRG may also contribute to the injured microenvironment through SASP release. Further investigation into these likely discrete populations would strengthen the overall understanding of senescence cell contribution to DRG pathology after peripheral injury.

In this study, we found that senescent neurons are a major cellular source of IL6 after injury in young or aged DRG. Release of IL6 in the DRG can impact excitability of nociceptors via ion channel modulation, resulting in pain[48–51]. We additionally showed that IL6 application increases evoked firing and, thereby, heightens excitability of senescent DRG neurons in aged animals. Production of cytokines such as IL6 in the DRG after injury has been attributed to infiltrating immune and glial cells, namely macrophages and Schwann cells, which subsequently contribute to neuronal sensitization[52,53]. Furthermore, although it has been reported that IL6-expressing neurons exist in the DRG after nerve injury[54], their function and the mechanism by which IL6 expression is induced remain unclear. We postulate senescence as a mechanism by which neurons produce IL6 as part of their SASP profile, which, in turn, acts on DRG neurons in an autocrine and/or paracrine manner[48], ultimately resulting in hyperexcitability and pain. Intriguingly, the expansion of $Trpv1^+$ nociceptors co-expressing both p21 and IL6 with age and after injury provided evidence that this particular population, highly implicated in pain sensation, can be impacted by such cytokine production. Clinical studies support aberrant DRG excitability contributing to pain, evidenced by the temporary effectiveness of peripheral anesthetics[55] or nerve blockade[56] in patients with chronic pain. Interestingly, we were able to detect an increased SenMayo signature in human DRG associated with pain states[25], providing preliminary evidence that senescence in the DRG may impact pain outcomes in humans as well.

To evaluate the functional contribution of cellular senescence to sensory dysfunction, we used the senolytic ABT263, a small-molecule drug that selectively targets senescent cells by acting on Bcl-2 anti-apoptotic pathways[34,35]. Other studies employed such an approach, demonstrating that administration of senolytics in a model of chemotherapy-induced peripheral neuropathy[57] or nerve injury[5,39,58] can improve behavioral outcomes, with only one recent study implicating DRG neurons[39]. Preserving sensation by eliminating sensory neurons may sound contradictory; however, correct timing of elimination (that is, before too many cells senesce) may enable preservation of overall primary sensory neuron numbers. For example, elimination of senescent cells supported overall survival of the many unaffected retinal ganglion cells in experimental ocular hypertension as well as cortical neurons in the context of Alzheimer's disease pathology[18,59].

Cellular senescence is implicated in a variety of age-related pathologies; our data now extend the importance of this process to the PNS and its dysfunction. We identify senescent DRG neurons as the cellular source of the pain-producing cytokine, IL6. Furthermore, these neurons contain highly excitable and IL6-responsive populations, emphasizing their potential contribution to overall DRG excitability and pain. Overall, we describe a susceptibility of the PNS to neuronal senescence with age or injury that may be a targetable mechanism to treat sensory dysfunction, such as chronic pain, particularly in aged populations.

Online content

Any methods, additional references, Nature Portfolio reporting summaries, source data, extended data, supplementary information, acknowledgements, peer review information; details of author contributions and competing interests; and statements of data and code availability are available at https://doi.org/10.1038/s41593-025-01954-x.

References

1. Melzer, D., Pilling, L. C. & Ferrucci, L. The genetics of human ageing. *Nat. Rev. Genet.* **21**, 88–101 (2020).
2. Millecamps, M. et al. The geriatric pain experience in mice: intact cutaneous thresholds but altered responses to tonic and chronic pain. *Neurobiol. Aging* **89**, 1–11 (2020).
3. Vincent, K., Dona, C. P. G., Albert, T. J. & Dahia, C. L. Age-related molecular changes in the lumbar dorsal root ganglia of mice: signs of sensitization, and inflammatory response. *JOR Spine* **3**, e1124 (2020).

4. Wang, S. & Albers, K. M. Behavioral and cellular level changes in the aging somatosensory system. *Ann. N. Y. Acad. Sci.* **1170**, 745–749 (2009).
5. Muralidharan, A. et al. Long-term male-specific chronic pain via telomere- and p53-mediated spinal cord cellular senescence. *J. Clin. Invest.* **132**, e151817 (2022).
6. Borghesan, M., Hoogaars, W. M. H., Varela-Eirin, M., Talma, N. & Demaria, M. A senescence-centric view of aging: implications for longevity and disease. *Trends Cell Biol.* **30**, 777–791 (2020).
7. Gorgoulis, V. et al. Cellular senescence: defining a path forward. *Cell* **179**, 813–827 (2019).
8. Baker, D. J. et al. Naturally occurring $p16^{Ink4a}$-positive cells shorten healthy lifespan. *Nature* **530**, 184–189 (2016).
9. Baker, D. J. et al. Clearance of $p16^{Ink4a}$-positive senescent cells delays ageing-associated disorders. *Nature* **479**, 232–236 (2011).
10. Xu, M. et al. Senolytics improve physical function and increase lifespan in old age. *Nat. Med.* **24**, 1246–1256 (2018).
11. Stein, G. H., Drullinger, L. F., Soulard, A. & Dulić, V. Differential roles for cyclin-dependent kinase inhibitors p21 and p16 in the mechanisms of senescence and differentiation in human fibroblasts. *Mol. Cell. Biol.* **19**, 2109–2117 (1999).
12. Jurk, D. et al. Postmitotic neurons develop a p21-dependent senescence-like phenotype driven by a DNA damage response. *Aging Cell* **11**, 996–1004 (2012).
13. Kang, C. et al. The DNA damage response induces inflammation and senescence by inhibiting autophagy of GATA4. *Science* **349**, aaa5612 (2015).
14. Herdy, J. R. et al. Increased post-mitotic senescence in aged human neurons is a pathological feature of Alzheimer's disease. *Cell Stem Cell* **29**, 1637–1652 (2022).
15. Dehkordi, S. K. et al. Profiling senescent cells in human brains reveals neurons with CDKN2D/p19 and tau neuropathology. *Nat. Aging* **1**, 1107–1116 (2021).
16. Fielder, E., von Zglinicki, T. & Jurk, D. The DNA damage response in neurons: die by apoptosis or survive in a senescence-like state? *J. Alzheimers Dis.* **60**, S107–S131 (2017).
17. Bussian, T. J. et al. Clearance of senescent glial cells prevents tau-dependent pathology and cognitive decline. *Nature* **562**, 578–582 (2018).
18. Musi, N. et al. Tau protein aggregation is associated with cellular senescence in the brain. *Aging Cell* **17**, e12840 (2018).
19. Herdy, J. R., Mertens, J. & Gage, F. H. Neuronal senescence may drive brain aging. *Science* **384**, 1404–1406 (2024).
20. Mailhot, B. et al. Neuronal interleukin-1 receptors mediate pain in chronic inflammatory diseases. *J. Exp. Med.* **217**, e20191430 (2020).
21. Jin, X. & Gereau, R. W. IV. Acute p38-mediated modulation of tetrodotoxin-resistant sodium channels in mouse sensory neurons by tumor necrosis factor-α. *J. Neurosci.* **26**, 246–255 (2006).
22. Goncalves Dos Santos, G., Delay, L., Yaksh, T. L. & Corr, M. Neuraxial cytokines in pain states. *Front. Immunol.* **10**, 3061 (2019).
23. Fang, D. et al. Interleukin-6-mediated functional upregulation of TRPV1 receptors in dorsal root ganglion neurons through the activation of JAK/PI3K signaling pathway: roles in the development of bone cancer pain in a rat model. *Pain* **156**, 1124–1144 (2015).
24. Mickle, A. D., Shepherd, A. J. & Mohapatra, D. P. Sensory TRP channels: the key transducers of nociception and pain. *Prog. Mol. Biol. Transl. Sci.* **131**, 73–118 (2015).
25. Saul, D. et al. A new gene set identifies senescent cells and predicts senescence-associated pathways across tissues. *Nat. Commun.* **13**, 4827 (2022).
26. Cohn, R. L., Gasek, N. S., Kuchel, G. A. & Xu, M. The heterogeneity of cellular senescence: insights at the single-cell level. *Trends Cell Biol.* **33**, 9–17 (2023).
27. Renthal, W. et al. Transcriptional reprogramming of distinct peripheral sensory neuron subtypes after axonal injury. *Neuron* **108**, 128–44 (2020).
28. Wang, K. et al. Single-cell transcriptomic analysis of somatosensory neurons uncovers temporal development of neuropathic pain. *Cell Res.* **31**, 904–918 (2021).
29. Tsujino, H. et al. Activating transcription factor 3 (ATF3) induction by axotomy in sensory and motoneurons: A novel neuronal marker of nerve injury. *Mol. Cell Neurosci.* **15**, 170–182 (2000).
30. Usoskin, D. et al. Unbiased classification of sensory neuron types by large-scale single-cell RNA sequencing. *Nat. Neurosci.* **18**, 145–153 (2015).
31. Shiers, S., Klein, R. M. & Price, T. J. Quantitative differences in neuronal subpopulations between mouse and human dorsal root ganglia demonstrated with RNAscope in situ hybridization. *Pain* **161**, 2410–2424 (2020).
32. Zhang, H. & Dougherty, P. M. Enhanced excitability of primary sensory neurons and altered gene expression of neuronal ion channels in dorsal root ganglion in paclitaxel-induced peripheral neuropathy. *Anesthesiology* **120**, 1463–1475 (2014).
33. Zheng, Y. et al. Deep sequencing of somatosensory neurons reveals molecular determinants of intrinsic physiological properties. *Neuron* **103**, 598–616 (2019).
34. Kirkland, J. L. & Tchkonia, T. Senolytic drugs: from discovery to translation. *J. Intern. Med.* **288**, 518–536 (2020).
35. Zhu, Y. et al. Identification of a novel senolytic agent, navitoclax, targeting the Bcl-2 family of anti-apoptotic factors. *Aging Cell* **15**, 428–435 (2016).
36. Georgakopoulou, E. A. et al. Specific lipofuscin staining as a novel biomarker to detect replicative and stress-induced senescence. A method applicable in cryo-preserved and archival tissues. *Aging* **5**, 37–50 (2013).
37. Yu, H. et al. Leveraging deep single-soma RNA sequencing to explore the neural basis of human somatosensation. *Nat Neurosci.* **27**, 2326–2340 (2024).
38. North, R. Y. et al. Electrophysiological and transcriptomic correlates of neuropathic pain in human dorsal root ganglion neurons. *Brain* **142**, 1215–1226 (2019).
39. Techameena, P., Feng, X., Zhang, K. & Hadjab, S. The single-cell transcriptomic atlas iPain identifies senescence of nociceptors as a therapeutical target for chronic pain treatment. *Nat. Commun.* **15**, 8585 (2024).
40. Sah, E. et al. The cellular senescence stress response in post-mitotic brain cells: cell survival at the expense of tissue degeneration. *Life* **11**, 229 (2021).
41. Sapieha, P. & Mallette, F. A. Cellular senescence in postmitotic cells: beyond growth arrest. *Trends Cell Biol.* **28**, 595–607 (2018).
42. Frade, J. M. & Ovejero-Benito, M. C. Neuronal cell cycle: the neuron itself and its circumstances. *Cell Cycle* **14**, 712–720 (2015).
43. Katchanov, J. et al. Mild cerebral ischemia induces loss of cyclin-dependent kinase inhibitors and activation of cell cycle machinery before delayed neuronal cell death. *J. Neurosci.* **21**, 5045–5053 (2001).
44. Demaria, M. et al. An essential role for senescent cells in optimal wound healing through secretion of PDGF-AA. *Dev. Cell* **31**, 722–733 (2014).
45. ElShamy, W. M., Fridvall, L. K. & Ernfors, P. Growth arrest failure, G1 restriction point override, and S phase death of sensory precursor cells in the absence of neurotrophin-3. *Neuron* **21**, 1003–1015 (1998).
46. Fischer, S. J., McDonald, E. S., Gross, L. & Windebank, A. J. Alterations in cell cycle regulation underlie cisplatin induced apoptosis of dorsal root ganglion neurons in vivo. *Neurobiol. Dis.* **8**, 1027–1035 (2001).

47. Admasu, T. D., Rae, M. & Stolzing, A. Dissecting primary and secondary senescence to enable new senotherapeutic strategies. *Ageing Res. Rev.* **70**, 101412 (2021).
48. Miller, R. J., Jung, H., Bhangoo, S. K. & White, F. A. Cytokine and chemokine regulation of sensory neuron function. *Handb. Exp. Pharmacol.* 417–449 (2009).
49. Obreja, O. et al. Fast modulation of heat-activated ionic current by proinflammatory interleukin 6 in rat sensory neurons. *Brain* **128**, 1634–1641 (2005).
50. Cunha, T. M. et al. A cascade of cytokines mediates mechanical inflammatory hypernociception in mice. *Proc. Natl Acad. Sci. USA* **102**, 1755–1760 (2005).
51. Jeevakumar, V. et al. IL-6 induced upregulation of T-type Ca^{2+} currents and sensitization of DRG nociceptors is attenuated by MNK inhibition. *J. Neurophysiol.* **124**, 274–283 (2020).
52. Cui, J. G., Holmin, S., Mathiesen, T., Meyerson, B. A. & Linderoth, B. Possible role of inflammatory mediators in tactile hypersensitivity in rat models of mononeuropathy. *Pain* **88**, 239–248 (2000).
53. Bolin, L. M., Verity, A. N., Silver, J. E., Shooter, E. M. & Abrams, J. S. Interleukin-6 production by Schwann cells and induction in sciatic nerve injury. *J. Neurochem.* **64**, 850–858 (1995).
54. St-Jacques, B. & Ma, W. Role of prostaglandin E2 in the synthesis of the pro-inflammatory cytokine interleukin-6 in primary sensory neurons: an in vivo and in vitro study. *J. Neurochem.* **118**, 841–854 (2011).
55. Richards, N. & McMahon, S. B. Targeting novel peripheral mediators for the treatment of chronic pain. *Br. J. Anaesth.* **111**, 46–51 (2013).
56. Hayek, S. M. & Shah, A. Nerve blocks for chronic pain. *Neurosurg. Clin. N. Am.* **25**, 809–817 (2014).
57. Acklin, S. et al. Depletion of senescent-like neuronal cells alleviates cisplatin-induced peripheral neuropathy in mice. *Sci. Rep.* **10**, 14170 (2020).
58. Du, J. et al. Astrocyte senescence-like response related to peripheral nerve injury-induced neuropathic pain. *Cell. Mol. Biol. Lett.* **28**, 65 (2023).
59. Rocha, L. R. et al. Early removal of senescent cells protects retinal ganglion cells loss in experimental ocular hypertension. *Aging Cell* **19**, e13089 (2020).

Methods

Animals

All animal procedures were approved by the Stanford University Administrative Panel on Laboratory Animal Care and the Institutional Animal Care and Use Committee (IACUC; 34760) in accordance with American Veterinary Medical Association guidelines and the International Association for the Study of Pain. All mice were housed 2–5 per cage maintained on a 12-hour light/dark cycle in a temperature-controlled environment (temperature: 68–74 °F; humidity: 30–70%) with ad libitum access to food and water. Young male and female mice used were 11–16 weeks old, wild-type C57BL/6J mice (The Jackson Laboratory, stock no. 00664). Aged male and female mice used were 20–24 months-old, wild-type C57BL/6JN mice (NIA Aged Rodent Colony). We did not note any sex differences in the expression of senescence markers and, therefore, combined male and female DRG throughout all analyses. Aged mice were pre-screened for abnormal masses and cataracts and were included in the study only if they appeared healthy.

Human samples

Use of human postmortem DRG received human subjects exemption from the Stanford University Institutional Review Board. Human postmortem DRG were obtained in collaboration with Donor Network West. Human lumbar L4 DRG tissues were obtained from two young female donors (age 32 years and 33 years) and two aged donors, one male and one female (both age 65 years). All patients died from stroke or head trauma.

SNI

To perform SNI surgery[60], mice were anesthetized with isoflurane, and a small incision was made over the left thigh. Blunt dissection was performed through the biceps femoris muscle to expose the sciatic nerve and its three branches (common peroneal, tibial and sural nerves). The common peroneal and tibial nerves were then ligated using an 5-0 nylon suture (Ethilon, ref. no. 1668G), and these nerves were then axotomized using small-sized spring scissors. The sural nerve was left intact (the 'spared nerve'). The incision was closed with surgical staples. After surgery, mice were monitored for the study period, which varies from 1 day to 16 weeks depending on the timepoint of interest. Controls used for qPCR experiments were sham surgery in which an incision was made followed by opening of muscle to reveal the nerve, without touching the nerve, followed by closure.

Senolytic administration

ABT263 (Navitoclax) (MedChemExpress, catalogue number HY-10087) was dissolved in 60% Phosol40PG, 30% PEG400 and 10% ethanol (EtOH) at a concentration of 12.5 mg ml^{-1} using brief water bath sonication and vortexing. Young and aged mice were briefly anesthetized with isoflurane before they were dosed by oral gavage at 100 mg kg^{-1} daily for 5 days, with a 2-day rest period, followed by a second 5-day daily dosing.

qPCR

Whole DRG were collected, homogenized using a 1-ml glass homogenizer (PYREX, catalogue number 7724-1) and placed in TRIzol reagent (Invitrogen, cat. no., 15596018). RNA was isolated using miRNeasy Mini kit (Qiagen, cat. no. 217004). The concentration and purity of RNA samples were determined using a NanoDrop 2000 (Thermo Fisher Scientific). RNA was reverse transcribed using a SuperScript VILO cDNA Synthesis Kit (cat. no. 11754-050). qPCR analysis was performed with PowerUp SYBR Green Master Mix (Thermo Fisher Scientific, cat. no. A25741) and run on an Applied Biosystems 7900HT or on an Applied Biosystems StepOnePlus. Appropriate no-reverse-transcriptase and no-template controls were used for each 384-well PCR reaction. The cycle conditions were as follows: 50 °C for 2 minutes, 95 °C for 2 minutes and then 40 cycles of 15 seconds at 95 °C and 1 minute at 60 °C. Dissociation analysis was performed at the end of each run to ensure specificity. qPCR primers used included: *p21* F: 5′-GTGAGGAGGAGCATGAATGGA-3′, R: 5′-GCACCTTTTATTCTGCTGGCAA-3′; *p16* F: 5′-GTGTGCATGACGTGCGG-3′, R: 5′-CACCTGAATCGGGGTACGAC-3′; *p53 (Trp53)* F: 5′-TCATCCCTCCCCTTTTCTGTC-3′, R: 5′-ATGGCGGGAAGTAGACTGGC-3′; *Il6* F: 5′-GCTACCAAACTGGATATAATCAGGA-3′, R: 5′-CCAGGTAGCTATGGTACTCCAGAA-3′; *Ccl2* F: 5′-AGCACCAGCCAACTCTCACT-3′, R: 5′-CGTTAACTGCATCTGGCTGA-3′; ms-*Tnfα* (Qiagen, PPM03113G); ms-*Il1β* (Qiagen, PPM03109F); housekeeping: *Tuba1a* F: 5′-GTGCATCTCCATCCATGTTG-3′, R: 5′-GTGGGTTCCAGGTCTACGAA-3′. Relative quantification of gene expression was performed using the $2^{-\Delta\Delta C_T}$ method[61].

Tissue preparation

Mice were anesthetized using pentobarbital (Vortech Pharmaceuticals, NDC 0298-9373-68, 150 mg kg^{-1} in 0.9% saline) and transcardially perfused with 5 ml of 1× PBS followed by 30 ml of 10% formalin solution (Thermo Fisher Scientific). Lumbar DRG tissues were dissected and placed temporarily in RNAlater solution at room temperature (Thermo Fisher Scientific) and then frozen in O.C.T. Compound (Sakura Finetek, catalogue number 4583) on dry ice and stored at −80 °C. Mouse DRG was sectioned at 14 µm and mounted onto SuperFrost Plus glass slides, dried for 1 hour and stored at −80 °C. Human lumbar DRG were obtained from organ donors who were de-identified before collection. Extracted tissues were flash frozen immediately on dry ice and stored in screw cap 15-ml conical tubes and stored at −80 °C. DRG were slowly embedded in O.C.T. on dry ice and sectioned at 20 µm onto SuperFrost Plus glass slides and stored at −80 °C.

Fluorescent in situ hybridization

Fluorescent in situ hybridization using an RNAscope Multiplex V2 Kit (ACDBio, catalogue number 323100) was performed to detect the RNA of senescence markers, cytokine and DRG neuronal markers (p21 (*Cdkn1a*), p16 (*Cdkn2a*), *IL6* and *Tprv1*). In brief, DRG tissues were isolated and processed as described above. DRG sections (14 µm) were mounted on glass slides and dried for 1 hour at room temperature and stored at −80 °C. On day 1 of RNAscope, slides were submerged in 10% formalin and incubated for 20 minutes at 4 °C. Slides were washed (1× PBS) and dehydrated (EtOH) as described in the ACD RNAscope user manual (UM 323100). Sections were incubated for 10 minutes in RNAscope hydrogen peroxide solution, washed in Millipore water and incubated in RNAscope Protease IV for 1 minute (human) or 5 minutes (mouse) at room temperature. Slides were incubated with appropriate RNAscope probes (mouse probes: Mm-IL6-C1, catalogue number 315891, Mm-Cdkn1a-C2, cat. no. 408551-C2, Mm-Cdkn2a-C3, cat. no. 411011-C3, Mm-Cdkn2a-tv2-C2, cat. no. 447491, Mm-Trpv1, cat. nos. 313331-C1 and 313331-C3; human probes: Hs-TRPV1-C1, cat. no. 415381, Hs-CDKN2A-C2, cat. no. 310181-C2, Hs-CDKN1A-C3, cat. no. 311401) at 40 °C in a Hybez II oven (ACDBio) for 2 hours and stored overnight in 5× SSC buffer at room temperature. On day 2, slides were incubated in Amp1, Amp2 and/or Amp3 solutions followed by HRP-C1, HRP-C2 and/or HRP-C3 as appropriate. In each round, TSA Vivid dye reagents (1:1,000; ACDBio, TSA Vivid 520 catalogue number 323271, TSA Vivid 570 catalogue number 323272, TSA Vivid 650 cat. no. 323273) and HRP blocker were used. Negative control probes (ACDBio, catalogue number 321838) were used to assess background levels of RNAscope signal.

Immunohistochemistry

For immunohistochemistry performed immediately after RNAscope protocol (dual labeling), slides were first washed in 1× PBS and blocked (10% normal donkey serum, 0.3% Triton-X 100, in PBS) for 1 hour at room temperature. Slides were incubated with rabbit anti-ATF3 (1:200; Novus Bio, catalogue number NBP1-85816) in 1% blocking solution in 1× PBS at 4 °C overnight. Slides were washed three times in 1× PBS for 5 minutes each, incubated with Alexa Fluor secondary antibodies

(1:1,000; donkey anti-rabbit-A488, Life Technologies, cat. no. A21206) and mounted with Fluoromount G with DAPI (Thermo Fisher Scientific, cat. no. 00-4959-52).

For CC3 immunostaining, mice were transcardially perfused as described, and DRG tissues were extracted and frozen in O.C.T. Slides were then blocked (5% normal donkey serum, 0.3% Triton-X 100, in PBS) for 1 hour at room temperature. Rabbit CC3 primary antibody (1:200; Cell Signaling Technology, catalogue number 9661) was incubated overnight at 4 °C. Slides were incubated with secondary antibody (1:1,000; donkey anti-rabbit Alexa Fluor 555, Life Technologies, catalogue number A31572) for 2 hours in the dark, washed and mounted with Fluoromount G with DAPI. Primary antibody controls (no-primary conditions) were used throughout to validate immuno-positive signal.

SA-β-gal activity assay

Mice were perfused with cold 1× PBS. L3–L5 DRG were extracted and mounted onto O.C.T. DRG were sectioned at 14 µm onto glass slides. Slides were removed from the freezer, and 1× of fixative solution provided by Senescence β-Galactosidase Staining Kit (Cell Signaling Technology, catalogue number 9860S) was added to the slides for 15 minutes. Slides were rinsed in PBS, and a wax barrier was drawn around the sections. Fresh β-Galactosidase Staining Solution at pH 6.1 was added to the slides and incubated at 37 °C for 22 hours. β-Galactosidase Staining Solution was removed, and slides were rinsed twice in PBS and twice in distilled water before mounting and imaging. Fiji version 2.9.0 software was used to outline the area of the DRG, and the percentage of positive SA-β-gal pixels in the area was acquired and normalized to area. Sections[5–10] were analyzed per mouse.

Neuron diameter analysis

Fluorescent TIFF images taken from RNAscope experiments that labeled *p21*, *p16*, *IL6* RNA and DAPI were used to measure diameters of neurons in both mouse and human DRG. Cells were then categorized according to their co-expression of markers *p21*, *p16* or *IL6*. Using Fiji version 2.9.0 software, the scale (µm) was appropriately set based on objective used in image. The longest end-to-end cell diameters, with the line centered through each neuron using the 'line segment tool'. The line was measured using 'Measure' as an output in µm unit.

ELISA assay

One-milliliter syringes were coated with heparin and used to withdraw approximately 0.8 ml of blood from anesthetized mice. Blood was centrifuged (1-ml tubes) at 2,000*g* at 4 °C for 10 minutes. The supernatant was removed, aliquoted and stored at −80 °C. IL6 plasma concentration levels were measured using an IL6 ELISA kit (Thermo Fisher Scientific, catalogue number KMC0061). Samples were tested in duplicate and diluted 1:2. The final concentration was corrected for the dilution factor. A VersaMax tunable microplate reader (Molecular Devices) was used to calculate optical density (OD) values at 450 nm. Data were analyzed with Boster Bio's 5PL regression model and subtracting the blank well's OD value from the sample's OD values (https://www.bosterbio.com/biology-research-tools/elisa-data-analysis-online).

DRG neuron dissociation and culture

Lumbar L3–6 DRG were excised from aged mice (24 months) after transcardial perfusion with 3 ml of 1× PBS (Corning, ref. no. 21-031-CV). DRG were placed into DMEM media supplemented with 10% FBS and penicillin–streptomycin (10 U ml^{-1}/10 µg ml^{-1}; Thermo Fisher Scientific, catalogue number 15070063) on ice during collection. DRG were then washed with HBSS and placed in 3 ml of warmed Dispase II (2.5 mg ml^{-1})/Collagenase A (1.25 mg ml^{-1}) and incubated at 37 °C shaking (200 r.p.m.) for 30 minutes (Sigma-Aldrich, catalogue number 10103578001, catalogue number D4693-1G). DRG were then washed with 5 ml of HBSS and placed in 1 ml of neurobasal media (Thermo Fisher Scientific, cat no. 10888022) supplemented with 5% FBS (Sigma-Aldrich, cat. no. F4135-500ML), 1× GlutaMAX (Gibco, cat. no. 35050061), 1× B-27 supplement (Thermo Fisher Scientific, cat. no. 10889038) and penicillin–streptomycin. DRG were then triturated approximately 4–6 times with a P1000 pipette, followed by a series of four fire-polished glass pipettes of decreasing bore size. Dissociated cells were filtered through a 40-µm sterile mesh filter. Cells were spun at 300*g* for 4 minutes and resuspended in supplemented neurobasal media without FBS for subsequent culture. Twenty-four-well culture plates containing sterilized glass coverslips were pre-coated with 1/30th mixture of Geltrex LDEV-Free Reduced Growth Factor Basement Membrane Matrix (Thermo Fisher Scientific, catalogue number A1413202) with neurobasal media and incubated for 2 hours at 37 °C. Coverslips were rinsed with neurobasal media and left to dry in the culture hood for 1 hour. Cells were plated in 1 ml of supplemented neurobasal media without FBS. Coverslips were collected for electrophysiology recordings 48 hours after plating.

Electrophysiology

For ex vivo recording preparations, all extracellular solutions in contact with live tissue were bubbled with a 95% O_2/5% CO_2 gas. Animals were deeply anesthetized with a ketamine/xylazine bolus and transcardially perfused with a sucrose-based dissection solution (containing in mM: 250 sucrose, 2.5 KCl, 25 $NaHCO_3$, 1 NaH_2PO_4, 6 $MgCl_2$, 0.5 $CaCl_2$ and 25 glucose). The vertebral column was removed and placed in dissection solution. The DRG were removed and stripped of epineurium. The tissue was transferred to collagenase (1 mg ml^{-1} in dissection solution) to incubate for 30 minutes at 35 °C to digest the perineurium. Recordings were performed in a chamber (RC-26GLP; Warner Instruments) within an upright microscope (Nikon Eclipse FN1) and secured with a platinum wire-based anchor, and tissue was constantly perfused with artificial cerebrospinal fluid (aCSF; composition in mM: 125 NaCl, 2.5 KCl, 25 $NaHCO_3$, 1.0 NaH_2PO_4, 1.0 $MgCl_2$, 2.0 $CaCl_2$ and 25 glucose). For in vitro (culture) preparations, coverslips were pre-incubated with either IL6 (50 ng ml^{-1} with carrier, prepared from 100 µg ml^{-1} stock solution in 0.1% BSA; R&D Systems, catalogue number 406-ML) or control media (with 0.00005% BSA) for 1 hour before recording, and aCSF containing the same concentration of either IL6 or control BSA was applied (29–32 °C). Coverslips were discarded 1 hour after transfer to the recording chamber. Patch pipettes were pulled (P-97; Sutter Instruments) from single-filament borosilicate glass capillaries (1.5 mm OD, 1.1 mm ID; Sutter Instruments) with resistances from 5 MΩ to 8 MΩ and filled with internal patch solution as follows (in mM): 120 potassium gluconate, 20 KCl, 165 2 $MgCl_2$, 2 Na_2ATP, 0.5 NaGTP, 20 HEPES, 0.5 EGTA, pH adjusted to 7.2–7.3 with KOH. Signals were amplified (Multiclamp 700B; Molecular Devices), digitized (Digidata 1440A; Molecular Devices), filtered with a 4-kHz Bessel and sampled at 10 kHz (pClamp 10.6 software; Molecular Devices). Liquid junction potentials (−14 mV) were corrected for (JPCalc software, P. Barry, University of New South Wales, Sydney, Australia; modified for Molecular Devices). In current clamp, depolarizing current steps were applied from resting membrane potential to determine excitability parameters. After recordings, images were taken of the neuron to estimate size (the average of two separate diameter measurements), and the cytoplasm was aspirated into the patch pipette for subsequent PCR. PCR was performed using primers for p16 (Mm.PT.58.42804808; Integrated DNA Technologies (IDT)), p21 (Mm.PT.58.5884610; IDT), IL6 (Mm.PT.58.10005566; IDT), GFAP (to determine glia presence in sample; Mm01253033_m1; Thermo Fisher Scientific) and Tubb3 (to confirm that neuronal tissue was sampled; Mm.PT.58.32393592; IDT) in combination with TaqMan Gene Expression Master Mix (Thermo Fisher Scientific, catalogue number 4369016). Samples were then subjected to real-time PCR with the same primers and the SuperScript III One-Step RT–PCR System with Platinum Taq DNA Polymerase (Thermo Fisher Scientific, catalogue number 12574018). UMAP (Python implementation from https://github.com/lmcinnes/umap) was performed to integrate and connect the high-dimensional neuronal parameters[33] in low-dimensional 2D

space. Training was performed using the train_test_split function from scikit-learn over 1,000 epochs. UMAP hyperparameters were as follows: number of neighbors = 5, minimum distance = 0.815, local connectivity = 2, random state = 42. Clusters were then estimated via HDBSCAN (Python implementation from https://github.com/scikit-learn-contrib/hdbscan/blob/master/docs/index.rst) with the following parameters: minimum cluster size = 4, cluster selection epsilon = 9, cluster selection method = 'eom' or Excess of Mass. Parameters were normalized for heatmap visualization using the following equation: (p − min(p)) / (max(p) − min(p)), where p is a vector containing all measurements of a given parameter.

Mechanical nociception assays

To evaluate mechanical reflexive hypersensitivity, we used a logarithmically increasing set of eight von Frey filaments (Stoelting), ranging in gram force from 0.007 g to 6.0 g. These were applied perpendicular to the plantar hindpaw with sufficient force to cause a slight bending of the filament. A positive response was characterized as a rapid withdrawal of the paw away from the stimulus filament within 4 seconds. Using the up-down statistical method[62], the 50% withdrawal mechanical threshold scores were calculated for each mouse and then averaged across the experimental groups.

Unweighting

An incapacitance device (IITC Life Science) was used to measure hindpaw unweighting. Mice were placed in the plexiglass apparatus with a ramp with the hindpaws resting on separate metal scale plates. Measurements were taken when the hindpaws were supporting the weight of the mouse with forepaws on the ramp. Each measurement was 4–6 seconds, and six consecutive measurements were taken at 60-second intervals. Six readings were averaged to calculate the bilateral hindpaw weight-bearing values. The calculation of weight bearing on the injured hindlimb was as follows: 2 × (L) / (L + R) × 100 to get percent weight bearing on injured (L, left) hindlimb.

Imaging/image analysis

All imaging was performed using a Keyence BZ-X810 fluorescence microscope (Keyence Corporation) using a ×40 objective (mouse DRG) or a ×20 objective (human DRG). Eight to 12 DRG sections were imaged per mouse and 3–5 DRG sections per human sample. Images were saved as stitched/full focus TIFF files using Keyence BZ-X800 Analyzer version 1.1.1.8. Fiji 2.9.0 was used for subsequent image processing and analysis. All images were similarly adjusted for brightness and contrast (across the entire image) per experiment, with no additional alterations made to the image. Lipofuscin signal was defined by strong autofluorescence signal across all channels (488 nm, 550 nm and 647 nm).

Quantification and statistical analysis

Measurements of cohort sizes were determined based on historical data from our laboratory using a power analysis to provide greater than 80% power to discover 25% differences with $P < 0.05$ between groups to require a minimum of four animals per group for all behavioral outcomes and two animals per group for RNAscope analyses. All experiments were randomized by cage and performed by a blinded researcher. Researchers remained blinded throughout histological, biochemical, electrophysiological and behavioral assessments. Groups were unblinded at the end of each experiment before statistical analysis. All data are expressed as the mean values ± s.e.m. Data distribution was assumed to be normal, but this was not formally tested. Data were collected using Excel version 2108. Statistical analysis was performed using GraphPad Prism version 10.0.2, Python or R, as described in Methods. Data were analyzed using two-tailed Student's *t*-test or Mann–Whitney tests, depending on the normality of the distribution, as indicated in the main text or figure captions, as appropriate. Combinations of male and female mice, young or aged, were used throughout the study. No data were excluded from analyses. In some cases, the different sections of the same DRG from the same mouse was used to detect multiple senescence markers for RNAscope analyses. DAPI nuclear stain was used to determine glial–neuronal boundary to carefully associate RNAscope puncta with neuronal cell bodies. For mouse DRG, neurons expressing RNA were quantified per probe set as: IL6$^+$ >5 puncta; p16$^+$ >10 puncta; p21$^+$ >20 puncta; Trpv1$^+$ >20 puncta. Human DRG neuron cutoffs for positive counted cells were as follows: IL6 >10 puncta, p16 >15 puncta, p21 >20 puncta, Trpv1 >20 puncta. Experimenter was blinded to age/sex/timepoint per experiment during RNAscope quantification. All counts were conducted assessing more than 800 total DRG neurons per experiment per biological replicate. No experiment presented in this study failed to replicate.

Transcriptomic analysis of existing datasets

Single-nucleus and single-cell RNA-seq datasets were acquired from the sources described below. Transcriptomic data were processed in Python 3.10 using scanpy-1.10.1, anndata-0.10.7, numpy-1.26.4, scipy-1.11.4, pandas-2.2.2 and statsmodels-0.14.2 software packages. Differential gene expression significance was calculated using the Wilcoxon rank-sum test. *P* values were false discovery rate (FDR) corrected using the Benjamini–Hochberg method. A gene is considered differentially expressed if the $\log_2$ fold change (FC) is greater than |0.6| and the adjusted *P* value is less than 0.05. To detect senescent cell populations, discrete counts and percentages of senescent cells were calculated using several binary signatures as described in each figure. A cell was only considered positive for a signature if it contained a nonzero expression of all positive genes in the signature and zero expression of all negative genes in the signature. For example, a cell would be considered positive for the signature CDKN2A$^+$LMNB1$^-$TOP2A$^-$ if it had nonzero expression of CDKN2A and zero expression of LMNB1 and TOP2A. For SenMayo gene set scoring, single-cell and single-nucleus data were log1p transformed, centered and scaled around the gene mean and variance, respectively, using scanpy. To address differences in basal expression in SenMayo genes between cell types and highlight the changes in SenMayo scoring for each cell type, the same scaling was performed for each annotated cell type from Renthal et al.[27] independently. Scoring performed on the North et al.[38] bulk RNA-seq data was also scaled in the same manner but across the dataset. Gene set scoring was performed using the scanpy score genes method[63]. Scores were assessed for individual cells. Displayed heatmaps show the mean gene set score per annotated subtype and model timepoint.

For analysis of Renthal et al.[27], we downloaded post-quality control (QC) raw count matrices from Gene Expression Omnibus (GEO) accession GSE154659 (158,785 nuclei). In addition to their pre-processing, we removed a small number of probable doublets using the 'scrublet' tool from the scanpy library (294 nuclei), leaving us with 158,758 nuclei. We restricted our analysis to the nuclei from the C57 mouse SpNT model and naive samples. This left us with 16,895 neuronal nuclei and 11,957 nonneuronal nuclei. For consistency, we used the cell type annotations provided by Renthal et al. Raw count data were normalized to counts per 10,000 for analysis.

For analysis of Wang et al.[28], we aligned raw count matrices from GEO accession GSE155622 (114,243 cells). Our QC process removed 11,595 cells that had fewer than 500 unique molecular identifiers (UMIs) or fewer than 500 unique genes detected in a cell, had greater than 25% of UMIs from mitochondrial genes, had greater than 10% of UMIs from MALAT1 or were determined likely to be a doublet. After QC, we had 102,648 cells left for analysis. For consistency, we are using the cell type annotations provided by Wang et al. Raw count data were normalized to counts per 10,000 for analysis.

For analysis of Yu et al.[37], we aligned raw count matrices from GEO accession GSE249746 (1,136 cells). Consistent with the Smart-Seq2 protocol, somewhat higher mitochondrial gene count ratios were

observed, but we chose not to remove any cells from the analysis. Raw count data were normalized to counts per 10,000 for analysis.

For analysis of North et al.[38] (https://apps.utdallas.edu/bbs/painneurosciencelab/sensoryomics/hdrgclinical/), bulk RNA-seq data in transcripts per million (TPM) and sample metadata were parsed from Supplementary Files 1 and 2 in the associated article. No additional normalization or post-processing was performed.

Reporting summary

Further information on research design is available in the Nature Portfolio Reporting Summary linked to this article.

Data availability

Data that support the findings of this study will be available on Dryad at https://doi.org/10.5061/dryad.fbg79cp5v (ref. 64) within 6 months of publication. We re-analyzed data from the following existing sources: Renthal et al. GEO accession GSE154659; Wang et al. GEO accession GSE155622; Yu et al. GEO accession GSE249746; and North et al. (https://apps.utdallas.edu/bbs/painneurosciencelab/sensoryomics/hdrgclinical/). Source data used to make all figures are available as Source Data files for main figures and extended data figures. Source data are provided with this paper.

Code availability

Publicly available code was implemented in Python for the UMAP (https://github.com/lmcinnes/umap) and HDBSCAN (https://github.com/scikit-learn-contrib/hdbscan) analyses. Figures in these analyses were generated using Matplotlib (https://matplotlib.org/) and Seaborn (https://seaborn.pydata.org/). All code used to re-analyze publicly available datasets and generate associated figures is posted at https://github.com/Tawfik-Lab/Donovan_Senescence_2024 and https://doi.org/10.5281/zenodo.14902120.

References

60. Decosterd, I. & Woolf, C. J. Spared nerve injury: an animal model of persistent peripheral neuropathic pain. *Pain* **87**, 149–158 (2000).
61. Livak, K. J. & Schmittgen, T. D. Analysis of relative gene expression data using real-time quantitative PCR and the $2^{-\Delta\Delta C_T}$ method. *Methods* **25**, 402–408 (2001).
62. Chaplan, S. R., Bach, F. W., Pogrel, J. W., Chung, J. M. & Yaksh, T. L. Quantitative assessment of tactile allodynia in the rat paw. *J. Neurosci. Methods* **53**, 55–63 (1994).
63. Wolf, F. A., Angerer, P. & Theis, F. J. SCANPY: large-scale single-cell gene expression data analysis. *Genome Biol.* **19**, 15 (2018).
64. Donovan, L. J. et al. Aging and injury drive neuronal senescence in the dorsal root ganglia. *Dryad* https://doi.org/10.5061/dryad.fbg79cp5v (2025).

Acknowledgements

We would like to thank G. Muwanga, A. Ram and A. Cortez for technical help and discussion during the course of this project. We acknowledge important technical help from L. Chen and B. Cao in training us in the post-recording PCR analysis. We also thank A. Nippert and H. Fuhrmann for helpful comments during paper preparation. We used BioRender software to prepare multiple schematics included in this paper. This work was supported by National Institutes of Health (NIH) grants (1R21AG075622 and RF1AG088052 to V.L.T., T32DA035165 to L.J.D., K99AR083486 to C.L.B., T32HL110952 to O.C.G. and R01DA011289 to J.A.K.), a Belgian American Educational Foundation fellowship to L.C. and a philanthropic donation from the Duan Family to V.L.T.

Author contributions

L.J.D. and V.L.T. conceived the study. L.J.D., C.L.B., S.F.B., A.M.L., J.A.K. and V.L.T. contributed to study design and methodology. L.J.D., C.L.B., S.F.B., L.C., A.P.L., L.H.H. and C.E.J. performed experiments and collected data. L.J.D., C.L.B., S.F.B., A.M.L., A.P. and O.C.G. contributed to formal analysis of data. L.J.D., C.L.B. and V.L.T. wrote the original draft, and S.F.B., A.M.L., A.P.L., L.H.H., C.E.J., O.C.G., L.D.L. and J.A.K. additionally contributed to review and editing of the final paper. M.Q., L.D.L., J.A.K. and V.L.T. supervised the study.

Competing interests

L.J.D. and V.L.T. declare that they are named inventors on a pending patent (PCT/US2024/061293) held by Stanford University related to the use of senolytics for pain. A.L., A.P. and M.Q. are employees of Rubedo Life Sciences, a small biotechnology start-up working on senolytics for the treatment of chronic psoriasis and systemic sclerosis. The other authors declare no competing interests.

Additional information

Extended data is available for this paper at https://doi.org/10.1038/s41593-025-01954-x.

Supplementary information The online version contains supplementary material available at https://doi.org/10.1038/s41593-025-01954-x.

Correspondence and requests for materials should be addressed to Lauren J. Donovan or Vivianne L. Tawfik.

Peer review information *Nature Neuroscience* thanks Marina Trombetta Lima, Mark Mattson, Theodore Price and the other, anonymous, reviewer(s) for their contribution to the peer review of this work.

https://doi.org/10.1038/s41593-025-01954-x

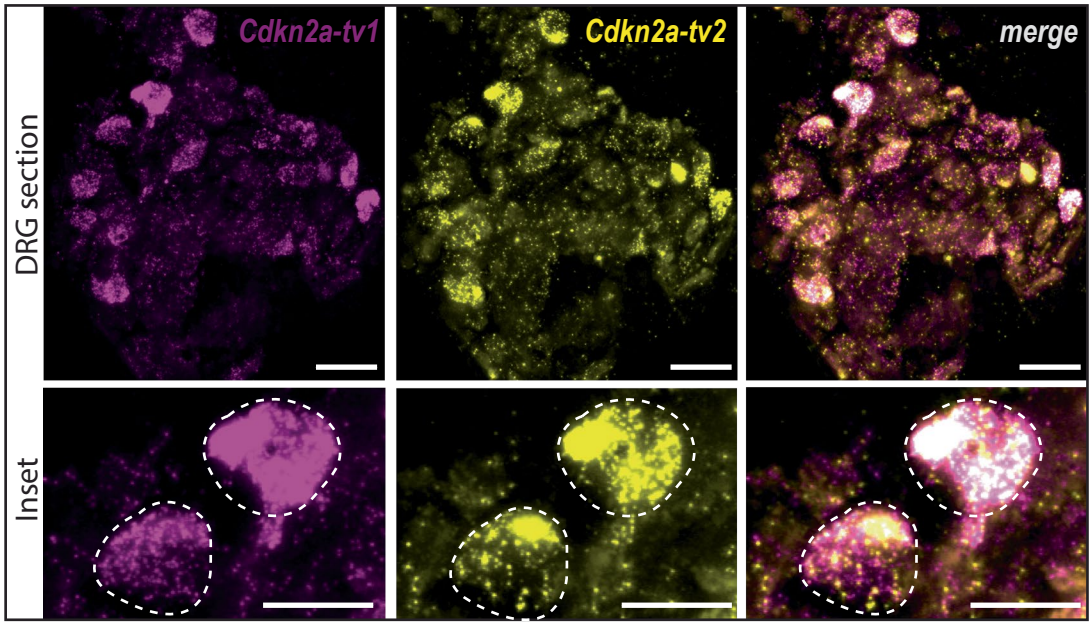

Extended Data Fig. 1 | Confirmation of p16^{INK4A}-specific RNA expression in the DRG. RNAscope using RNA probes spanning exons encoding both p16^{INK4A} and p19^{ARF} protein (*Cdkn2a-tv1*). *Cdkn2a-tv2* RNA probe spans exons specific to p16^{INK4A} protein. Individual primary sensory neurons outlined in inset images. Complete cellular co-localization of the two *Cdkn2a* variant probes in mouse lumbar DRG sections confirm p16-specific expression in mouse lumbar DRG neurons. Scale bar of upper panels are 25 µm. Scale bars of inset are 15 µm.

https://doi.org/10.1038/s41593-025-01954-x

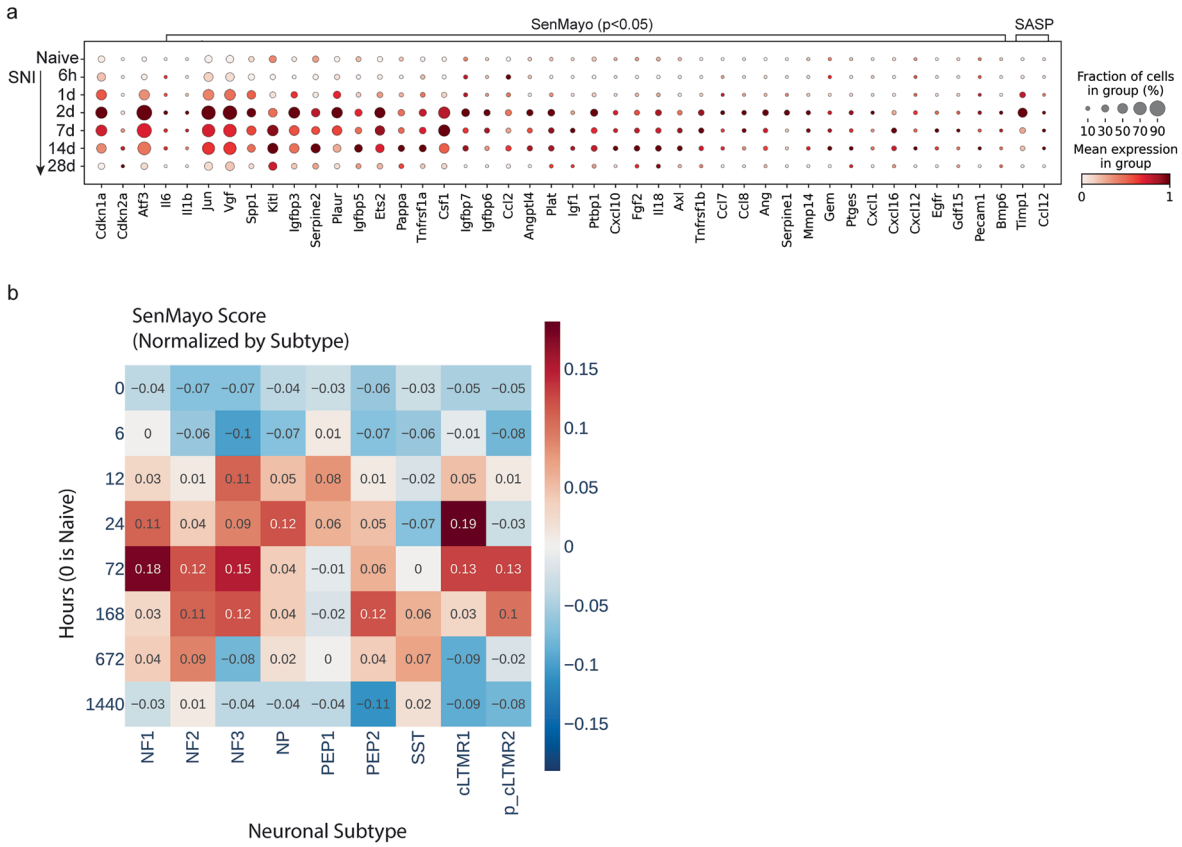

Extended Data Fig. 2 | Senescence marker gene expression patterns in DRG neurons post nerve-injury. a, Re-analysis of Wang et al.[28]. RNA-sequencing dataset from young adult mouse DRG. Dot plot displays changes in senescence marker gene expression following spared nerve injury (SNI). Genes under SenMayo subgroup are all significantly increased post-injury (at least one time point) (see Supplementary Table 3). **b**, Re-analysis of Renthal et al.[27]. RNA-sequencing dataset from young adult mouse DRG. Heatmap represents changes in SenMayo gene expression in DRG neuronal subtypes following sciatic nerve transection (ScNT). (see Supplementary Table 4).

https://doi.org/10.1038/s41593-025-01954-x

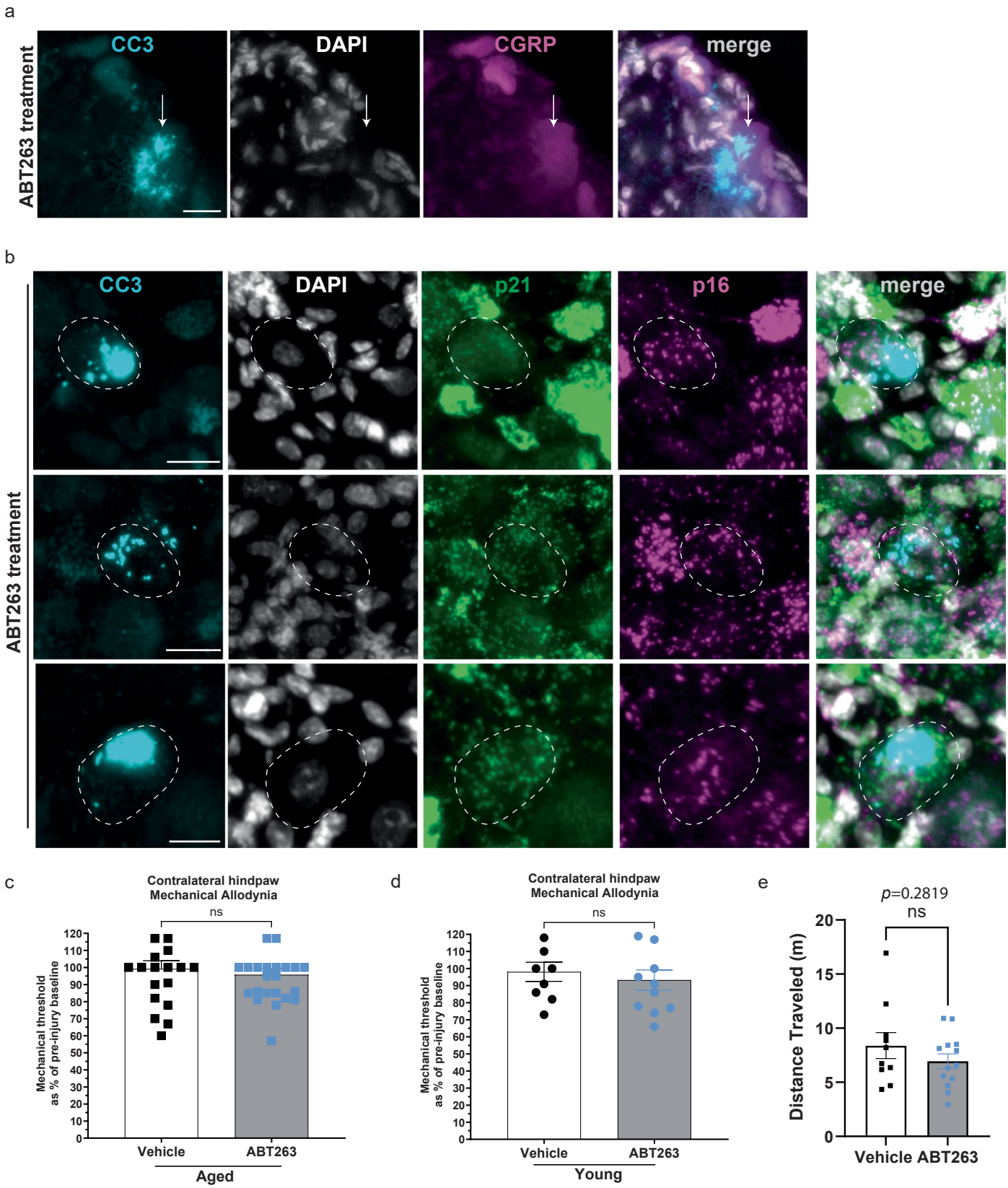

Extended Data Fig. 3 | See next page for caption.

https://doi.org/10.1038/s41593-025-01954-x

Extended Data Fig. 3 | Senolytic treatment induces senescent neuron apoptosis and does not alter normal sensory function. **a**, Immunohistochemistry showing co-localization of cleaved caspase-3 (CC3) apoptotic marker with neuronal marker (CGRP) and nuclei (DAPI) in the DRG post-ABT263 treatment. Scale bars 20 µm. **b**, Co-localization of CC3 (immunohistochemistry) with *p21* and *p16* (RNAscope) in DRG neurons post-ABT263 treatment. Positive neurons outlined. Top panel row represent neuron co-positive for CC3 and p16, while bottom to panel rows show examples of triple positive neurons. Scale bars 20 µm. **c,d**, The mechanical threshold of the contralateral (uninjured) hindlimb was measured after application of senolytic ABT263 or vehicle control in aged (**c**) and young (**d**) mice at Day19 post-treatment (n = 21 aged vehicle-treated mice, n = 24 aged ABT263-treated mice; n = 9 young vehicle-treated mice, n = 11 young ABT263-treated mice; two-tailed unpaired t-test, $p = 0.8562$ (aged mice), $p = 0.5858$ (young mice)). **e**, Open field analysis of aged mice treated with or without ABT263. (n = 10 vehicle-treated, 13 ABT263-treated aged mice, two-tailed unpaired t-test, $p = 0.2819$). All data are mean values ± SEM.

https://doi.org/10.1038/s41593-025-01954-x

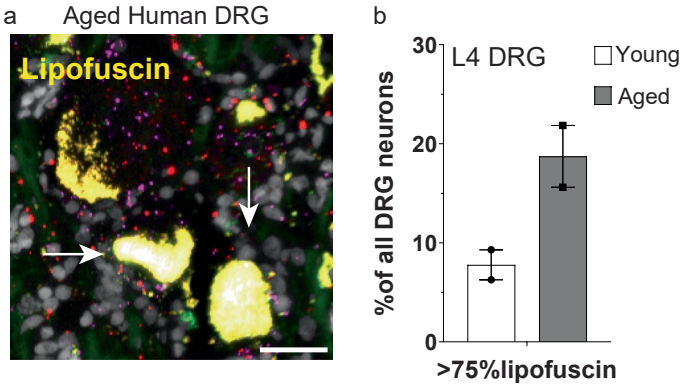

Extended Data Fig. 4 | Increased percentage of human DRG neurons filled with lipofuscin with age. a, Representative neurons in aged (65yo) human DRG with accumulated lipofuscin, a marker of senescence. Example of neuron either mostly filled (*left arrow*) or completely filled (*right arrow*). Scale bar is 10 µm. **b**, Quantification of DRG neurons whose cell bodies were greater than 75% occluded by lipofuscin as a percentage of all DRG neurons in young and aged human DRG (n = 2 young (32 & 33yo female); n = 1 aged male and n = 1 aged female (each 65yo) DRG. Lipofuscin signal is defined by strong autofluorescence signal across all channels (488 nm, 550 nm, 647 nm) which presents as a bright yellow/white signal in overlay. Data are mean values ± SEM.

https://doi.org/10.1038/s41593-025-01954-x

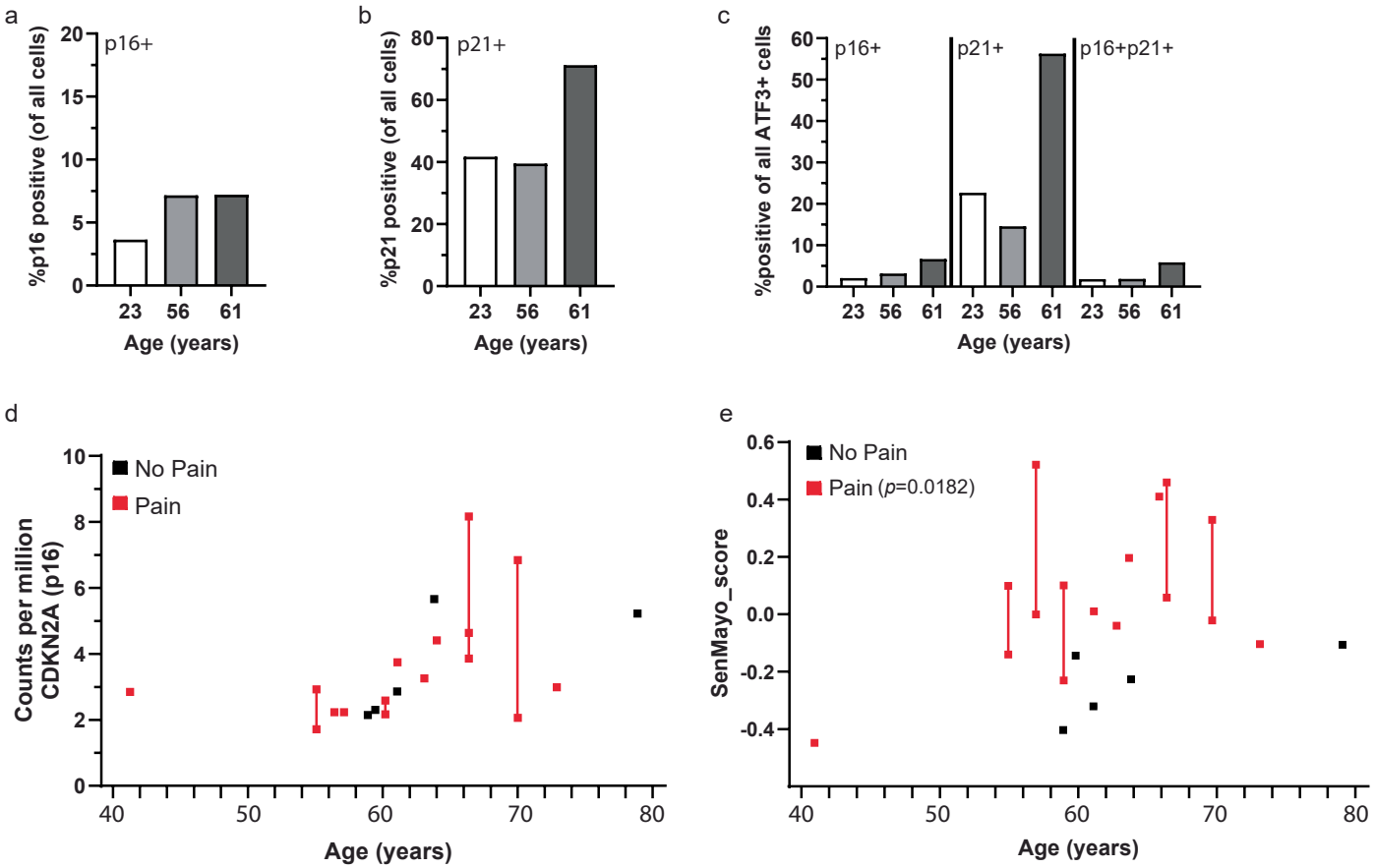

Extended Data Fig. 5 | Confirmation of human DRG senescence with age and in painful conditions using existing RNA-sequencing datasets. a-c, Re-analysis of Yu et al.[37] single-soma human DRG RNAseq dataset. Bar graphs represent the percent positive p16 (*CDKN2A*) cells (**a**) and p21 (*CDKN1A*) cells (**b**) of all DRG cells, which are also negative for *LMNB1*, *MKI67*, *TOP2A* to filter out any proliferating and otherwise non-senescent cells. **c**, Percent of *ATF3*+ neurons which are co-positive for either *p21* and/or *p16* senescence markers. **d,e**, Re-analysis of North et al.[38] human DRG bulk RNAseq dataset for expression of p16 (*CDKN2A*) (**d**) or SenMayo gene set (**e**) across multiple ages using DRG samples taken from patients either with associated pain (red) or without pain (black). Significant correlation found for *CDKN2A* expression with age (Spearman correlation, coefficient= 0.612, $p = 0.00321$). Significant association of SenMayo gene expression in pain DRG samples (t-test, $p = 0.0182$, see Supplementary Table 1).

https://doi.org/10.1038/s41593-025-01954-x

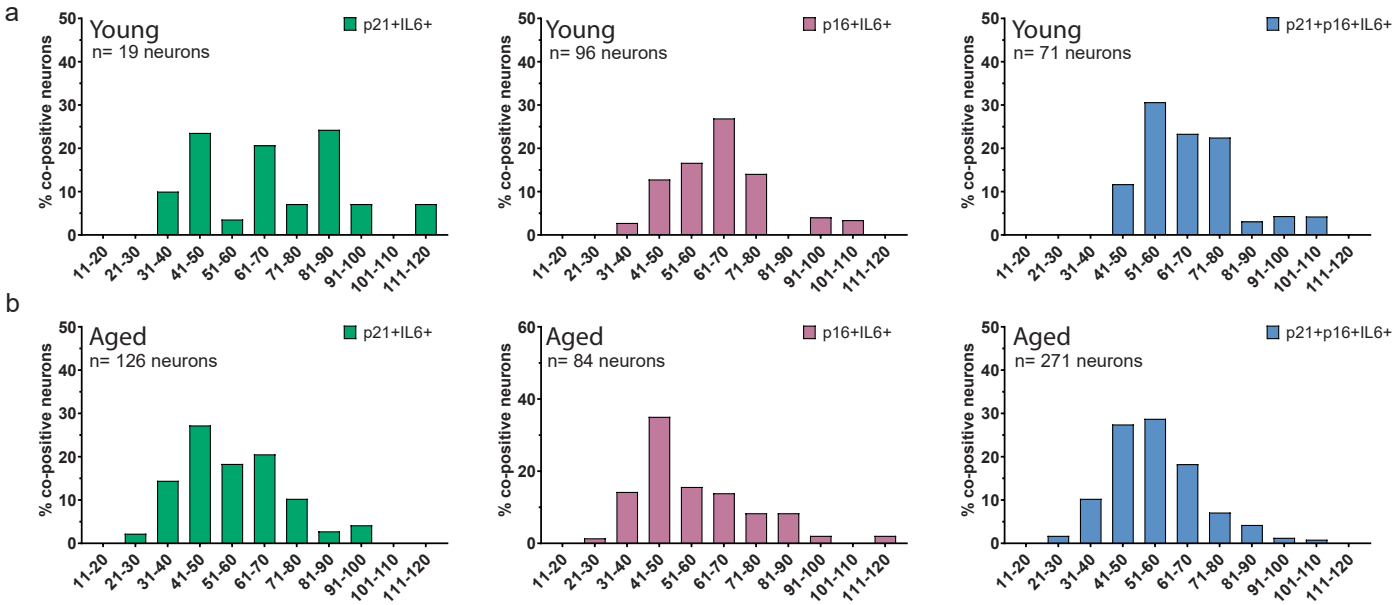

Extended Data Fig. 6 | SASP-expressing senescent neuron diameters in young and aged human DRG. Cell diameters (μm) of human DRG neurons co-expressing either *p21* + *IL6* + , *p16* + *IL6* + , or *p21* + *p16* + *IL6* + , as a percent of total neurons counted in each population in young (**a**) and aged (**b**) DRG (n = 2 young female (33yo and 32yo) DRG: n = 19 *p21* + *IL6* + DRG neurons, n = 96 *p16* + *IL6* + DRG neurons, n = 71 *p16* + *p21* + *IL6* + DRG neurons; n = 2 aged male and female (65yo) DRG: n = 126 *p21* + *IL6* + DRG neurons, n = 84 *p16* + *IL6* + DRG neurons, n = 271 *p16* + *p21* + *IL6* + DRG neurons).

nature portfolio

Corresponding author(s): Vivianne L. Tawfik

Last updated by author(s): February 25, 2025

Reporting Summary

Nature Portfolio wishes to improve the reproducibility of the work that we publish. This form provides structure for consistency and transparency in reporting. For further information on Nature Portfolio policies, see our Editorial Policies and the Editorial Policy Checklist.

Statistics

For all statistical analyses, confirm that the following items are present in the figure legend, table legend, main text, or Methods section.

n/a	Confirmed	
☐	☒	The exact sample size (*n*) for each experimental group/condition, given as a discrete number and unit of measurement
☐	☒	A statement on whether measurements were taken from distinct samples or whether the same sample was measured repeatedly
☐	☒	The statistical test(s) used AND whether they are one- or two-sided *Only common tests should be described solely by name; describe more complex techniques in the Methods section.*
☐	☒	A description of all covariates tested
☐	☒	A description of any assumptions or corrections, such as tests of normality and adjustment for multiple comparisons
☐	☒	A full description of the statistical parameters including central tendency (e.g. means) or other basic estimates (e.g. regression coefficient) AND variation (e.g. standard deviation) or associated estimates of uncertainty (e.g. confidence intervals)
☐	☒	For null hypothesis testing, the test statistic (e.g. *F*, *t*, *r*) with confidence intervals, effect sizes, degrees of freedom and *P* value noted *Give P values as exact values whenever suitable.*
☒	☐	For Bayesian analysis, information on the choice of priors and Markov chain Monte Carlo settings
☐	☒	For hierarchical and complex designs, identification of the appropriate level for tests and full reporting of outcomes
☒	☐	Estimates of effect sizes (e.g. Cohen's *d*, Pearson's *r*), indicating how they were calculated

Our web collection on statistics for biologists contains articles on many of the points above.

Software and code

Policy information about availability of computer code

Data collection	Excel v2108 was used for data collection and GraphPad v10.0.2 was used for data collection and generation of graphs. Biorender.com (latest update Jan 13,2025) was used to generate schematic figures. Fluorescent microscopy images were taken on a Keyence BZ-X800 (2018 Keyence Corporation).
Data analysis	Fluorescent microscopy images were processed (stitched and full focus) using Keyence BZ-X800 Analyzer v1.1.1.8. Fiji 2.9.0 was used for subsequent image processing and analysis. GraphPad v10.0.2 was used for statistical analyses of experimental data. Publicly available code was implemented in Python for the UMAP (https://github.com/lmcinnes/umap) and HDBSCAN (https://github.com/scikit-learn-contrib/hdbscan) analyses. Figures in these analyses were generated using Matplotlib (https://matplotlib.org/) and Seaborn (https://seaborn.pydata.org/). Transcriptomic data was processed in python 3.10 using scanpy-1.10.1, anndata-0.10.7, numpy-1.26.4, scipy-1.11.4, pandas-2.2.2, statsmodels-0.14.2 software packages. Differential gene expression significance was calculated using the Wilcoxon rank-sum test, as provided by the SciPy software package. All code used to reanalyze publicly available datasets and generate associated figures will be posted at: https://github.com/Tawfik-Lab/ Donovan_Senescence_2024 and https://doi.org/10.5281/zenodo.14902120.

For manuscripts utilizing custom algorithms or software that are central to the research but not yet described in published literature, software must be made available to editors and reviewers. We strongly encourage code deposition in a community repository (e.g. GitHub). See the Nature Portfolio guidelines for submitting code & software for further information.

Data

Policy information about availability of data

All manuscripts must include a data availability statement. This statement should provide the following information, where applicable:

- Accession codes, unique identifiers, or web links for publicly available datasets
- A description of any restrictions on data availability
- For clinical datasets or third party data, please ensure that the statement adheres to our policy

Data that support the findings of this study will be available on Dryad at the following location https://doi.org/10.5061/dryad.fbg79cp5v within 6 months of publication.

Research involving human participants, their data, or biological material

Policy information about studies with human participants or human data. See also policy information about sex, gender (identity/presentation), and sexual orientation and race, ethnicity and racism.

Reporting on sex and gender	Human lumbar L4 DRG tissues were used in this study taken from de-identified post-mortem organ donors. Three female (32yo, 33yo, 65yo) and one male (65yo) donor was collected from in this study.
Reporting on race, ethnicity, or other socially relevant groupings	Human lumbar L4 DRG tissues were obtained from one white female donor (age 33), one Hispanic or Latino female donor (age 32), one male donor whose ethnicity was not reported (age 65), and one white female donor (age 65).
Population characteristics	Two donors were categorized as 'young' (32 & 33yo), and two donors were catagorized as 'aged' (65yo) in this study.
Recruitment	Donors were post-mortem. Human lumbar L4 DRG tissues were obtained from young female donors (age 32&33yo), and two aged donors one male, one female (both age 65). All patients died from stroke or head trauma.
Ethics oversight	Use of human post-mortem DRG received Stanford University Institutional Review Board for human subjects exemption.

Note that full information on the approval of the study protocol must also be provided in the manuscript.

Field-specific reporting

Please select the one below that is the best fit for your research. If you are not sure, read the appropriate sections before making your selection.

☒ Life sciences ☐ Behavioural & social sciences ☐ Ecological, evolutionary & environmental sciences

For a reference copy of the document with all sections, see nature.com/documents/nr-reporting-summary-flat.pdf

Life sciences study design

All studies must disclose on these points even when the disclosure is negative.

Sample size	Cohort sizes were determined based on historical data from our laboratory using a power analysis to provide >80% power to discover 25% differences with p<0.05 between groups to require a minimum of 4 animals per group for all behavioral outcomes. Power analysis was used to determine sample sizes for molecular analyses (RNAscope).
Data exclusions	No data were excluded from analyses.
Replication	Each experiment was replicated in separate cohorts of mice. Experiments using RNAscope detection of p21, p16, IL6, and Trpv1 were replicated in separate experiments and with several different secondary dyes. All data and trends were consistent in each replicated experiment. No experiment failed to replicate the results presented in this study.
Randomization	For all experiments presented, mice were allocated into experimental groups in a random manner, with each cage of mice representing an experimental block.
Blinding	Experimenters were blinded to group allocation during data collection for behavior analyses. Experimenters were blinded to age/sex/timepoint for RNAscope quantification cell counts. In all electrophysiology experiments, the identity of each neuron was unknown to the electrophysiologist during experimentation.

Reporting for specific materials, systems and methods

We require information from authors about some types of materials, experimental systems and methods used in many studies. Here, indicate whether each material, system or method listed is relevant to your study. If you are not sure if a list item applies to your research, read the appropriate section before selecting a response.

Materials & experimental systems

n/a	Involved in the study
☐	☒ Antibodies
☒	☐ Eukaryotic cell lines
☒	☐ Palaeontology and archaeology
☐	☒ Animals and other organisms
☒	☐ Clinical data
☒	☐ Dual use research of concern
☒	☐ Plants

Methods

n/a	Involved in the study
☒	☐ ChIP-seq
☒	☐ Flow cytometry
☒	☐ MRI-based neuroimaging

Antibodies

Antibodies used

Primary antibodies used: Rabbit anti-ATF3 (Novus Bio, Cat#NBP1-85816) and Rabbit anti-Cleaved-caspase-3 (Cell Signaling Technology, Cat#9661). Secondary antibodies used included: AlexaFluor secondary antibodies (Donkey anti-rabbit-A488, LifeTechnologies, Cat# A21206 and Donkey anti-rabbit Alexa-555, LifeTechnologies, Cat#A31572).

Validation

For ATF3 primary antibody validation, Novus Bio confirmed reactivity in human and mouse tissues among other species and validated applications such as IHC used in this study. Further validation by both Genetic and Biological strategies is noted on supplier website. Details include: 1) Genetic Strategy Validation- Expression of the target protein is compared before and after knockout or knockdown using CRISPR/CAS9 or siRNA/shRNA. If protein expression following knockout or knockdown is substantially reduced, then antibody specificity is ensured. and 2) Biological Strategies Validation- These strategies use defined biological or chemical modulation of protein expression to demonstrate antibody specificity to the target protein. The data is compared across multiple cell lines including positive and negative expressing cells, and multiple species.

For Cleaved caspase-3 antibody validation, Cell Signaling Technology confirmed: Cleaved Caspase-3 (Asp175) Antibody detects endogenous levels of the large fragment (17/19 kDa) of activated caspase-3 resulting from cleavage adjacent to Asp175. This antibody does not recognize full length caspase-3 or other cleaved caspases. This antibody detects non-specific caspase substrates by western blot. Non-specific labeling may be observed by immunofluorescence in specific sub-types of healthy cells in fixed-frozen tissues (e.g. pancreatic alpha-cells). Nuclear background may be observed in rat and monkey samples.

Primary antibody controls (no-primary conditions) were used throughout to validate immuno-positive signal.

Animals and other research organisms

Policy information about studies involving animals; ARRIVE guidelines recommended for reporting animal research, and Sex and Gender in Research

Laboratory animals

All animal procedures were approved by the Stanford University Administrative Panel on Laboratory Animal Care and Institutional Animal Care and Use Committee (IACUC; 34760) in accordance with American Veterinary Medical Association guidelines and the International Association for the Study of Pain. C57BL/6J male and female mice at 11-16 weeks old and C57BL/6JN male and female mice at 20-24 months old from NIA aged rodent colony (C57BL/6JN). All mice were housed 2-5 per cage maintained on a 12-hour light/dark cycle in a temperature-controlled environment (Temp:68-74F; Humidity:30-70%) with ad libitum access to food and water.

Wild animals

The study did not involve wild animals.

Reporting on sex

Male and female mice were used throughout the study as described.

Field-collected samples

The study did not involve samples collected from the field.

Ethics oversight

Stanford University Administrative Panel on Laboratory Animal Care and Institutional Animal Care and Use Committee (IACUC; 34760)

Note that full information on the approval of the study protocol must also be provided in the manuscript.

Plants

Seed stocks

Report on the source of all seed stocks or other plant material used. If applicable, state the seed stock centre and catalogue number. If plant specimens were collected from the field, describe the collection location, date and sampling procedures.

Novel plant genotypes

Describe the methods by which all novel plant genotypes were produced. This includes those generated by transgenic approaches, gene editing, chemical/radiation-based mutagenesis and hybridization. For transgenic lines, describe the transformation method, the number of independent lines analyzed and the generation upon which experiments were performed. For gene-edited lines, describe the editor used, the endogenous sequence targeted for editing, the targeting guide RNA sequence (if applicable) and how the editor was applied.

Authentication

Describe any authentication procedures for each seed stock used or novel genotype generated. Describe any experiments used to assess the effect of a mutation and, where applicable, how potential secondary effects (e.g. second site T-DNA insertions, mosiacism, off-target gene editing) were examined.